COMPUTER SCIENCE

Genetically supported targets and drug repurposing for brain aging: A systematic study in the UK Biobank

Fan Yi[1], Jing Yuan[2], Judith Somekh[3], Mor Peleg[3], Yi-Cheng Zhu[2]*, Zhilong Jia[4]*, Fei Wu[1]*, Zhengxing Huang[1]*

Brain age gap (BAG), the deviation between estimated brain age and chronological age, is a promising marker of brain health. However, the genetic architecture and reliable targets for brain aging remains poorly understood. In this study, we estimate magnetic resonance imaging (MRI)–based brain age using deep learning models trained on the UK Biobank and validated with three external datasets. A genome-wide association study for BAG identified two unreported loci and seven previously reported loci. By integrating Mendelian Randomization (MR) and colocalization analysis on eQTL and pQTL data, we prioritized seven genetically supported druggable genes, including *MAPT*, *TNFSF12*, *GZMB*, *SIRPB1*, *GNLY*, *NMB*, and *C1RL*, as promising targets for brain aging. We rediscovered 13 potential drugs with evidence from clinical trials of aging and prioritized several drugs with strong genetic support. Our study provides insights into the genetic basis of brain aging, potentially facilitating drug development for brain aging to extend the health span.

INTRODUCTION

Delaying aging is an efficient approach to forestall disease and extend health span, and a 2% delay in aging could lead to health care cost savings of $7.1 trillion over 50 years (*1*, *2*). A growing amount of evidence suggests that brain aging, a key ingredient of human aging, is associated with decreased mental and physical fitness and with an increased risk of neurodegeneration and mortality (*3*). There is a general consensus that the trajectories of brain aging differ substantially among individuals due to differences in genetic factors, lifestyles, environmental factors, and chronic diseases of the patient (*4*). In this sense, the brain age gap (BAG), the difference between the estimated brain age and chronological age of a subject, may provide a promising indicator of aging-related brain function. Elucidating genetic factors explaining the BAG may identify the genetically supported targets and facilitate potential therapeutic opportunities to prevent, slow down, or even reverse brain aging, probably extending the health span of individuals (*5*, *6*).

Brain aging can be revealed by magnetic resonance imaging (MRI) of individuals (*7*), and machine learning models developed on MRIs for brain biological age estimation have surged in the past few decades (*8*, *9*). These models mainly used MRI scans of cognitively healthy participants, combined with supervised learning algorithms, such as simple fully convolutional network (SFCN) (*10*, *11*), VGGNet (*11*–*13*), EfficientNet (*14*), DenseNet (*15*), global-local transformer (GLT) (*16*), and ResNet (*17*–*19*), to train a regression model between the extracted brain imaging embedding features and the subject's chronological age (*17*). Then, the learned model can be applied to independent MRI test data to infer the brain age of unseen subjects. Furthermore, genetic factors have been investigated to understand the underlying cause of BAG from multiple perspectives (*4*, *17*, *20*–*23*). Previous genome-wide association studies (GWASs) for BAG have identified a set of associated genes (*17*, *22*–*26*), including Microtubule Associated Protein Tau (*MAPT*), involved in modulating the stability of axonal microtubules, and Runt-related transcription factor 2 (*RUNX2*), involved not only in regulation of bone cell differentiation and cell proliferation but also in hippocampal functions such as learning and memory (*27*). Also, the heritability of BAG, as estimated with single-nucleotide polymorphisms (SNPs) using linkage disequilibrium (LD) score regression (LDSC) (*28*), is ~0.2 (*17*, *25*). A recent study attempted to uncover the causal relations between BAG and common brain disorders using Mendelian randomization (MR) (*4*). Their analysis indicated weak evidence of a causal influence of Alzheimer's disease (AD) and bipolar disorder (BIP) on higher BAG.

Although existing studies emphasize the polygenic architecture of brain aging, genetically supported drug target studies of brain aging, as a tool to anticipate the effect of drug action on brain aging, are incredibly lacking (*29*). Identifying BAG-associated loci could provide a resource for reasoning targets of abnormal brain aging. Wen *et al.* (*22*, *23*) explored the relevance of BAG to diseases and identified potentially repositionable drugs for aging-related diseases directly using GWAS identified genes and their associated drug-disease networks. Rosoff *et al.* (*30*) identified drug targets for healthy aging via MR for clinical biomarkers and risk factor using multivariate GWAS. As reported in the ChEMBL database (*31*), there are 45 drugs in clinical trials related to aging. Partridge *et al.* (*32*) and Kulkarni *et al.* (*33*) have systematically reviewed the most promising agents to maintain health for longer periods and to slow down aging. These include drugs for managing diabetes [Sodium/Glucose cotransporter 2 (SGLT)-2 inhibitors, metformin, and acarbose], mammalian target of rapamycin (mTOR) inhibitors (rapamycin and its analogs), drugs for management of hypertension (angiotensin-converting enzyme inhibitors and angiotensin receptor blockers), and nonsteroidal anti-inflammatory drugs. A genetically supported drug target MR analysis can benefit in inferring whether and, in certain cases, in what direction a drug that acts on the protein (whether an antagonist, agonist, activator, or inhibitor) will alter brain aging. Finan *et al.* (*34*) redefined the druggable genes as whose encoded proteins are extracellular proteins, or targeted by drugs or drug-like

[1]College of Computer Science and Technology, Zhejiang University, Hangzhou, China. [2]Department of Neurology, Peking Union Medical College Hospital, Peking Union Medical College, Chinese Academy of Medical Sciences, Beijing, China. [3]Department of Information Systems, University of Haifa, Haifa, Israel. [4]Medical Innovation Research Division of Chinese PLA General Hospital, Beijing, China.
*Corresponding author. Email: zhuyc@pumch.cn (Y.-C.Z.); jiazhilong@plagh.org (Z.J.); wufei@zju.edu.cn (F.W.); zhengxing.h@gmail.com (Z.H.)

molecules (licensed or in clinical phase), and grouped them into three tiers of druggable genes, corresponding to their positions in the drug development stages. Effective yet unexploited drug targets might exist for the prevention or treatment of accelerated brain aging, and they could be identified through their causal associations with proteins in blood or brain tissues.

This study systematically investigates the genetic architecture of brain aging and identifies a set of druggable targets (*34*) by assessing their causal relevance for BAG (Fig. 1). We began by estimating brain age using seven state-of-the-art deep learning models, using MRI data from 38,961 UK Biobank (UKB) (*35*) participants and validating these models on three external datasets. The three-dimensional vision transformer (3D-ViT) (*36*) model outperformed others in brain age estimation and was used to measure BAG in subsequent analyses. Next, we conducted GWAS on genetic data from 31,520 UKB individuals to identify genomic regions associated with

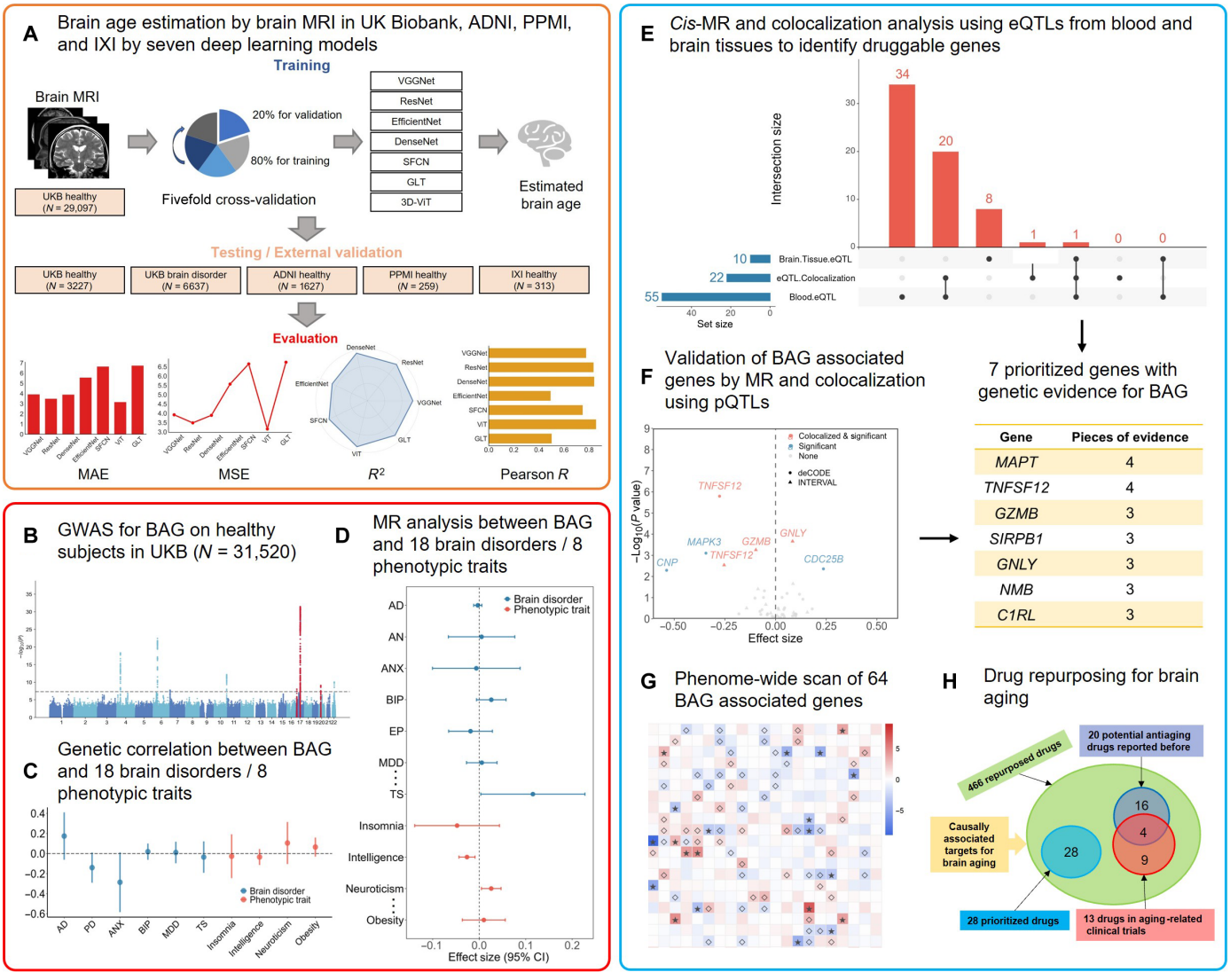

Fig. 1. Study design. (**A**) Brain age estimation: We trained seven deep learning models for brain age estimation using the UKB dataset on 29,097 healthy participants, validated using 3227 healthy and 6637 brain disorder subjects, In addition, we performed external validation using MRI data from 1627 CN subjects from ADNI, 259 healthy participants from PPMI, and 313 healthy participants from IXI. Models were evaluated using the four metrics: MAE, MSE, R^2, and Pearson *R*. (**B**) GWASs for BAG: We conducted a series of GWASs on 31,520 healthy participants with genotypes data from UKB, excluding brain disorder subjects to avoid confounding effects. These studies aimed to investigate the genetic basis of BAG, considering both continuous values and BAG within case-control groups. (**C** and **D**) Causal effects of BAG: To uncover potential health impacts of BAG, we conducted genetic correlation and Mendelian Randomization (MR) to investigate the causal effect of BAG on 18 brain disorders and eight phenotypic traits. CI, confidence interval. (**E**) Drug-target MR and colocalization for identifying druggable genes: We performed *cis*-MR and colocalization analysis using *cis*-eQTL to identify genes whose expression is associated with BAG. We found 64 druggable genes that could serve as potential therapeutic targets. (**F**) Further validation of BAG-associated genes: pQTL-based MR and colocalization further prioritized seven targets with strong genetic evidence. (**G**) Phenome-wide scan for the BAG-associated druggable genes: To explore the broader effects of the 64 identified druggable genes, we conducted a comprehensive phenome-wide scan to investigate their potential associations with 44 different traits to uncover potential therapeutic implications beyond brain aging. (**H**) Drug repurposing for brain aging: We explored the potential for repurposing existing drugs for the treatment of brain aging.

BAG. Through MR and genetic association analyses, we explored the relationships between BAG and 18 brain disorders, as well as eight phenotypic traits. Although most causal relationships were nonsignificant, we identified a significant causal effect of BAG on intelligence. We then identified 64 druggable genes using "drug target MR" (*37*–*39*) and colocalization analysis with eQTL and pQTL data. Seven druggable genes—*MAPT*, *TNFSF12*, *GZMB*, *SIRPB1*, *GNLY*, *NMB*, and *C1RL*—emerged as strong causal candidates for brain aging. A phenome-wide scan further explored their associations with 44 additional traits, helping to rationalize these targets. Inspired by Finan's work (*34*), we performed drug repurposing and identified 13 potential drugs, supported by clinical trial evidence on aging, which target the identified druggable genes. Our integrated pipeline—combining multimodal (MRI and omics) data, deep learning, MR, and colocalization analyses—provides a comprehensive framework for identifying druggable targets for brain aging and could aid in the translation of these findings into drug development for brain aging.

RESULTS

UKB participants with MRI data

We collected a total of 38,961 subjects with their T1-weighted MRI data from UKB, consisting of 32,324 non-brain disorder subjects and 6637 subjects recorded with brain damage or neurodegenerative and psychiatric disorders. These MRI data have been preprocessed and registered to the MNI152 standard space. On average, the enrolled subjects were 64 (SD 7.65) years old, and 20,417 (52.54%) were women. Subjects with brain damage and brain disorders mainly consists of 32 patients with AD, 81 patients with Parkinson's disease (PD), 132 with demyelination (DEM), 1152 with anxiety disorder (ANX), 1404 with major depressive disorder (MDD), 72 with BIP, 17 with obsessive-compulsive disorder (OCD), 21 with post-traumatic stress disorder (PTSD), 23 with schizophrenia (SCZ), 432 with cerebral vascular accident (CVA), 261 with epilepsy (EP), 600 with sleeping disorder (SLD), and the remaining with other types of brain disorders. Information on brain disorders was extracted based on the main diagnosis of the International Classification of Diseases, 10th Revision (ICD-10) from UKB (table S1).

3D-ViT outperforms other models in MRI-based brain age estimation

We used T1-weighted MRI data from UKB, consisting of 29,097 subjects without any brain disorders, to estimate brain age. We used seven state-of-the-art deep learning models, namely, SFCN, ResNet, EfficientNet, VGGNet, DenseNet, GLT, and 3D-ViT, whose neural network structure is shown in Fig. 2A. Among these models, 3D-ViT, we proposed to be applied in brain age estimation, demonstrated the highest performance in brain age estimation in terms of four regression metrics: mean absolute error (MAE), mean squared error (MSE), *R*-squared (R^2) score, and Pearson correlation coefficient (r) (Fig. 2B). Specifically, the overall performance of 3D-ViT, measured by fivefold cross validation, exhibited an overall performance with a MAE of 2.64 and r value of 0.90 on the training data (Fig. 2, B and C, and fig. S1, A to E). When evaluating the independent testing dataset, consisting of 3227 healthy participants and 6637 patients with brain disorders, 3D-ViT consistently achieved favorable results. For healthy participants, it yielded a MAE of 2.60 and a Pearson r value of 0.91 (Fig. 2D). In subjects with brain disorders, 3D-ViT demonstrated a significantly higher MAE of 2.78 ($P = 2.53 \times 10^{-43}$ for BAGs compared with healthy participants) and a Pearson r value of 0.89 (fig. S1F). Furthermore, the MAE remained consistent when analyzing the sex-separated dataset. Specifically, for the training data, the MAE was 2.58 for females and 2.71 for males, whereas for the testing data, it was 2.63 for females and 2.82 for males (fig. S2).

External validation confirms robustness for the 3D-ViT model

To demonstrate the generalizability of the used BAG estimation model, we conducted external validation using healthy participants extracted from three additional datasets: Alzheimer's Disease Neuroimaging Initiative (ADNI) ($N = 1627$), Information eXtraction from Images (IXI) ($N = 313$), and Parkinson's Progression Markers Initiative (PPMI) ($N = 259$). The six models trained on the UKB dataset were fine-tuned on the output layer for each external validation dataset. As a result, 3D-ViT consistently outperformed the other six models and obtained remarkable performance on the external validation datasets (Fig. 2B). Specifically, on the ADNI dataset, 3D-ViT achieved a MAE of 2.99 and a Pearson r value of 0.76 (Fig. 2E and fig. S3). On the PPMI dataset, it achieved a MAE of 3.44 and a Pearson r value of 0.91 (fig. S4). Last, on the IXI dataset, 3D-ViT achieved a MAE of 3.61 and a Pearson r value of 0.85 (fig. S5). Given its superior performance on both UKB and external validation datasets, 3D-ViT was selected as the optimal model for estimating BAG, which was then used in the subsequent analyses.

Brain disorders, cognition, and lifestyle factors reveal BAG differences

We observed a significant difference in BAG between subjects with brain disorders and healthy participants in the UKB dataset (Fig. 2F). Specifically, subjects with AD (average BAG = 2.59, $P = 5.00 \times 10^{-6}$), DEM (3.69, $P = 2.05 \times 10^{-38}$), and SCZ (2.12, $P = 0.0015$) exhibited larger discrepancies in BAG, indicating the reliability of our model from another perspective because subjects with brain disorders tend to have a larger BAG, as expected. In addition, we identified significant changes in most cognitive scores of the cognitive function tests with the increases of BAG (fig. S6), further demonstrating the reliability of the proposed brain age estimation model. Furthermore, our findings revealed that males, smokers, and individuals with either higher or lower body mass index (BMI) tend to have a greater BAG compared to females, nonsmokers, and individuals with a normal BMI, respectively (fig. S7).

Saliency maps identify key brain regions for BAG estimation

We used the 3D-ViT model and conducted an analysis to identify the most influential neuroimaging signatures of T1-MRI in brain age estimation. To accomplish this, we used saliency maps to highlight the contribution and relevance of each brain region in differentiating subjects based on BAG. Our findings revealed interesting insights about the relevance of specific brain regions in estimating the biological age of subjects. The lentiform nucleus and posterior limb of internal capsule regions showed notable relevance for estimating the brain biological ages of subjects (Fig. 2G). We also observed weak correlations in the thalamus, corpus callosum, and caudate nucleus regions (Fig. 2G), indicating that these regions may be associated with brain aging.

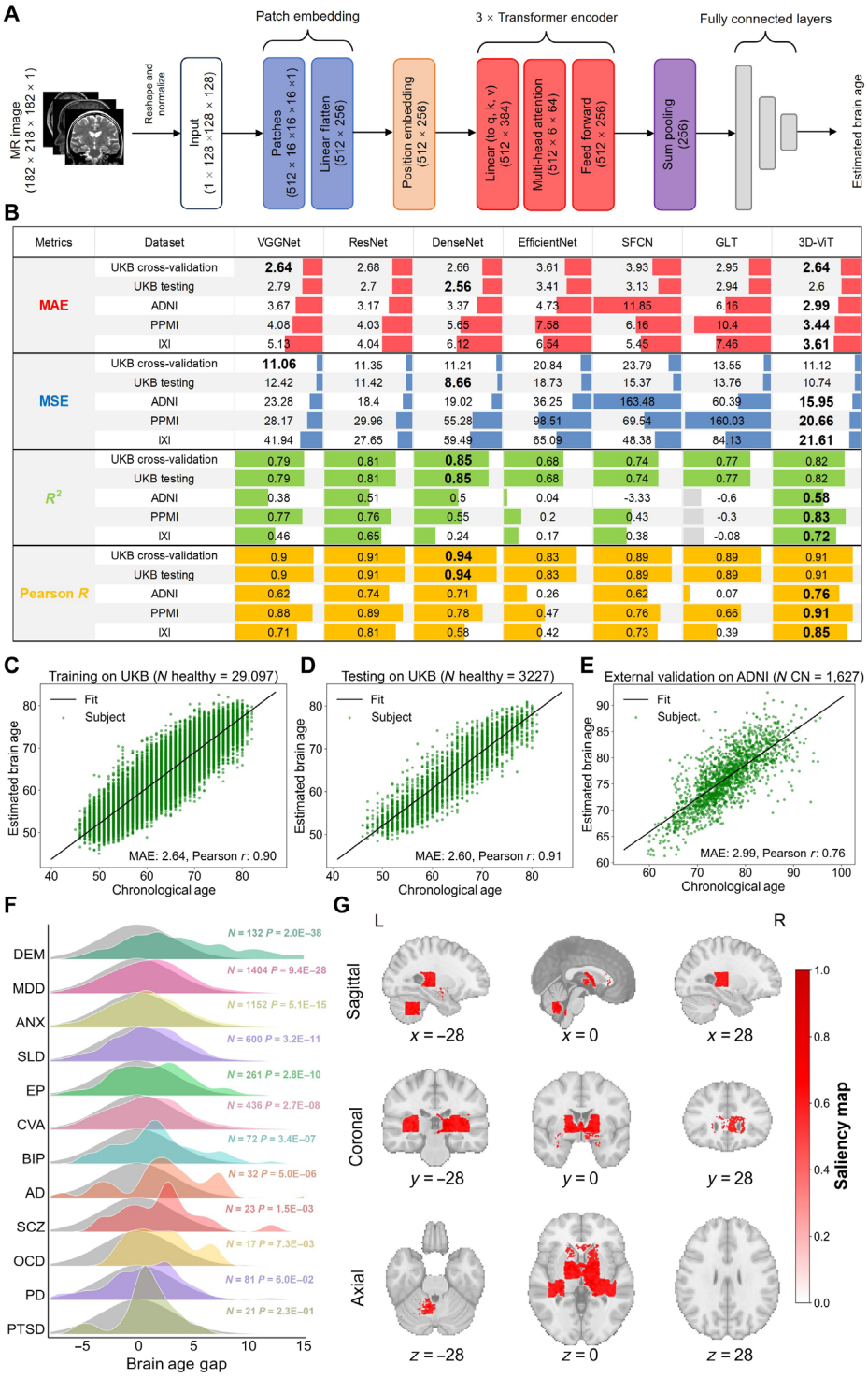

Fig. 2. Brain age estimation. (**A**) Overall neural network structure of the proposed 3D-ViT for brain age estimation, consisting of input layer, patch embedding, position embedding, triple transformer encoder, sum pooling, and fully connected layers. (**B**) Performance comparison of the seven models for brain age estimation on four regression metrics. (**C** to **E**) Brain age estimation performance on non-brain disorder subjects (green dots) in the training, testing data of the UKB dataset, and external validation on the CN subjects (green dots) in the ADNI dataset. (**F**) Statistical comparison of BAG distribution between subjects with 12 different brain diseases and subjects without any brain disorders in the UKB dataset. (**G**) Saliency maps of brain regions of participants without any brain disorders, from slices in three directions: sagittal, coronal, and axial. Saliency maps were calculated based on the voxel-wised gradient of the test data with darker red representing more important regions. The lentiform nucleus and posterior limb of internal capsule regions were highly relevant. AD, Alzheimer's disease; ANX, anxiety disorder; BIP, bipolar disorder; CVA, cerebral vascular accident; DEM, demyelination; EP, epilepsy; MDD, major depressive disorder; OCD, obsessive-compulsive disorder; PD, Parkinson's disease; PTSD, post-traumatic stress disorder; SCZ, schizophrenia; SLD, sleep disorder.

GWASs reveal genetic loci associated with brain aging

We conducted a series of GWASs for brain aging, including BAG with continuous values and BAG categorized into case-control groups (i.e., BAG > μ versus BAG ≤ μ and BAG < −μ versus BAG ≥ −μ, where μ = 1, 2, 3, 4, and 5 years, respectively, and the highest 25% of BAG versus the lowest 25% of BAG). The genotyped data was available for 31,520 subjects without any brain disorders in the extracted UKB dataset. To evaluate the statistical power of each GWAS, we calculated genetic heritability by LDSC, the number of independent genome-wide-significant loci, and other statistics. Our findings revealed that GWAS using BAG with continuous values exhibited the highest statistical power among all GWASs we implemented (figs. S8 to S20, and table S2). Hence, we chose to use the obtained GWAS results using BAG with continuous values of BAG for subsequent analyses.

We identified nine independent lead SNPs in eight genomic loci that exhibit significant associations with continuous BAG (Fig. 3, A and B; figs. S21 to S29; and table S3). The genomic inflation factor (λ) is 1.09, indicating no substantial genomic inflation (Fig. 3B). The identified SNPs were annotated using Ensembl Variant Effect Predictor (*40*), as shown in data S14. Our study replicated previously reported BAG-associated genes, such as *RUNX2*, *INPP5A*, *CRHR1*, and *PICK1*, and identified unreported associated genes, such as *TP53* and *NKX2-2*. In the GWAS results, a high LD block (Fig. 3A and table S3) located at the 17q21.31 polymorphism highlighted significant genomic regions related to brain aging. For example, *CRHR1*, with the lead SNP rs62056932 at 17q21.31 (Fig. 3C and fig. S26), plays a crucial role in synaptic loss and memory deficits (*41*, *42*), whereas *NSF* (lead SNP rs199534 at 17q21.31; fig. S27), a vesicle-fusing ATPase (adenosine triphosphatase), is associated with AD (*43*). Most of them are highly expressed in brain tissues (Fig. 3D). In addition, previously reported associations with BAG were observed for genes such as *RUNX2* (lead SNP rs2819861; Fig. 3C and fig. S22), *KLF3* (lead SNP rs13144836 at 4p14; fig. S21), *PICK1* (lead SNP rs738443 at 22q13.1; fig. S29), and *INPP5A* (lead SNP rs35831787 at 10q26.3; fig. S24) (*4*, *17*). Notably, we identified two previously unreported associations between *TP53*, *NKX2-2*, and BAG. *TP53* (lead SNP rs62062581 at 17p13.1, $P = 9.82 \times 10^{-9}$; Fig. 3C and fig. S25) has been associated with brain aging in zebra fish (*44*), and modulation of the p53-MDM2 axis has been linked to aging (*45*). *NKX2-2* (lead SNP rs73129833 at 20p11.22, $P = 8.43 \times 10^{-10}$; fig. S28), a transcription factor, plays critical role in in the maintenance of glucose tolerance and β cell function (*46*). Furthermore, the distinct expression patterns of the identified genes across the 54 tissue types from the GTEx v8 project (Fig. 3D) reinforced the understanding that BAG involves coordinated physiological processes in both the brain and peripheral systems, corroborating previous findings by Leonardsen *et al.* (*4*).

BAG shows limited causal associations with brain disorders/traits

We investigated the genetic heritability of BAG and the genetic correlations between BAG and both 18 brain disorders (which encompassed neurodegenerative disorders, psychiatric disorders, stroke, etc.) and eight phenotypic traits using LDSC with their GWAS summary results (figs. S30 and S31). The total SNP heritability (h^2) estimate for BAG was 0.186 (SE = 0.026; table S2). We observed a nominal genetic correlation between BAG and stroke ($r = 0.17$, SE = 0.074, $P = 0.025$, FDR-corrected $P = 0.27$) and small vessel stroke ($r = 0.27$, SE = 0.12, $P = 0.033$, FDR-corrected $P = 0.27$). However, no significant associations were detected after false discovery rate (FDR) correction.

Then, we conducted a bidirectional two-sample MR analysis to explore the causal direction and effect between BAG and 18 common brain disorders using five different MR methods. In the forward MR analysis (i.e., BAG as exposure), we observed slightly causal effects of BAG on PD and Tourette syndrome (TS) (fig. S32). In the reverse MR analysis (i.e., brain disorders as exposure), we observed causal effects of multiple sclerosis (MS) and AD on BAG (fig. S33). However, none of them exhibited significant correlations after FDR correction (figs. S32 and S33). Moreover, we performed a bidirectional two-sample MR analysis to examine the causal direction and effect between BAG and eight phenotypic traits using five different MR methods (figs. S34 and S35). Our findings revealed significant causal effects of BAG solely on intelligence among all phenotypic traits, whereas nonsignificant causal effects of these phenotypic traits on BAG were observed.

Cis-eQTL analyses identify 64 potential druggable genes for BAG

We conducted a comprehensive *cis*-MR analysis by integrating GWAS summary data for BAG with *cis*-eQTL data, consisting of blood eQTLs from eQTLGen and brain tissue eQTLs from the PsychENCODE consortia. The aim was to prioritize druggable and causal genes associated with BAG. After excluding nondruggable genes, we identified 2682 druggable genes from blood eQTLs and 2915 genes from brain tissue eQTLs within a 250-kb range for *cis*-MR analysis. Overall, we found that the expression of 64 druggable genes was causally associated with BAG (FDR-corrected $P < 0.05$; Fig. 4, A and B, and data S15 and S16), with no evidence of significant horizontal pleiotropy. Specifically, 55 genes in blood were causally associated with BAG, whereas 10 genes in brain tissues were associated with BAG. Notably, *MAPT* showed a significant causal effect on BAG in both blood and brain tissues (Fig. 4, A and B). The enriched Reactome pathways with the 64 druggable genes include programmed cell death, platelet signaling and aggregation, extracellular matrix organization, cell surface interactions at the vascular wall, and apoptosis (Fig. 4F).

We performed colocalization analysis to further refine the BAG-associated targets among the identified causal genes for BAG. This analysis was conducted to determine whether the genetic associations with both gene expression and BAG shared the same causal variant. When both MR and colocalization results demonstrated significance, it suggested a higher likelihood of the protein being a viable drug target (*47*). Consequently, we identified 22 druggable genes (*MAPT*, *NMB*, *CYP2D6*, *NOS3*, *GDF15*, *ITGAM*, *TNFRSF10A*, *TUBB*, *MPL*, *ALPL*, *MMP24*, *TNFSF13*, *INSL3*, *HSD3B7*, *FZD3*, *KLHL24*, *BMP8B*, *CELSR2*, *MUC4*, *MLKL*, *TSPEAR*, and *SDR42E1*) that were associated and colocalized with BAG (Table 1). These genes exhibited compelling evidence of association from both MR and colocalization analyses (PPH4 > 0.75; Fig. 4, A and B, and data S16 and S17).

pQTL analyses provide further genetic evidence

The application of MR and colocalization analysis using pQTLs allows for the validation of genetically supported targets for brain aging at the protein level. To this end, we conducted a search for pQTL data pertaining to the identified druggable genes in two large-scale

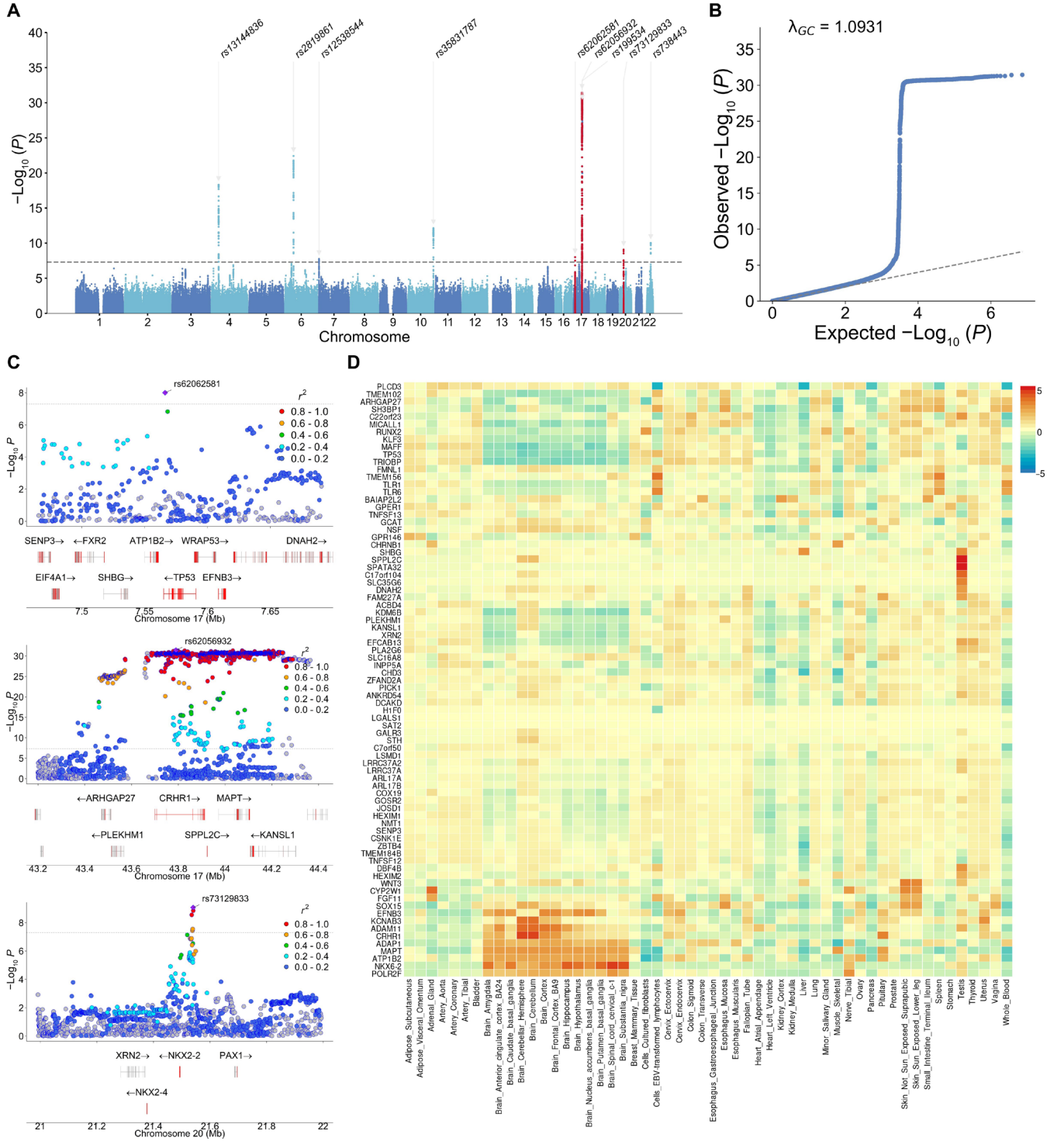

Fig. 3. GWAS results for BAG. (**A**) Manhattan plot for the GWAS on BAG. The *x* axis represents the chromosomes, whereas the *y* axis represents the $-\log_{10}(P)$ values for each genetic variant. The GWAS Manhattan plot displays the lead SNPs in each region, along with their corresponding rs-IDs. Loci with red dots (the two unreported loci and the top loci) are zoomed with annotation below. (**B**) The QQ plot assesses the results of the GWAS conducted on BAG. (**C**) The region plot showcases the associated regions of the lead SNPs. Genes located within each region are depicted below. (**D**) The heatmap displays the expression levels of the annotated genes across various tissues from the GTEx v8 study. The colors indicate the average normalized expression level (with zero mean across tissues) in each tissue.

Table 1. Evidence supporting the BAG causally associated druggable genes. The listed 41 genes have at least two significant pieces of evidence in xQTL (eQTL and pQTL) MR and colocalization analysis (37 genes) or are targeted by potentially antiaging drugs associated with aging-related clinical trials or previously reported (4 genes). The genes in the column are ordered according to the number of the pieces of evidence and the number of associated antiaging drugs. In terms of druggability tiers, Tier 1 represents proteins associated with approved drugs and drugs in clinical development. Tier 2 includes proteins closely related to drug targets or with associated drug-like compounds. Tier 3 comprises extracellular proteins and members of key drug target families. ✓, pass; ✗, fail; blank, unable to test; No. drugs, the number of drugs that targeting the genes; No. antiaging drugs, the number of potential antiaging drugs associated with aging-related clinical trials or previously reported.

Genes	Druggability Tier	Sig. in MR using eQTLs		Colocalization with eQTL		Sig. in MR using pQTLs		Colocalization with pQTL		No. drugs	No. antiaging drugs	Pieces of evidence
		Blood	Brain tissues	Blood	Brain tissues	Interval	deCODE	Interval	deCODE			
MAPT	Tier 1	✓	✓	✓	✗		✗		✓	43	6	4
TNFSF12	Tier 1	✓		✗		✓	✓	✗	✓	1	0	4
GZMB	Tier 2			✗		✓		✓	✗	0	0	3
SIRPB1	Tier 3A			✗				✓	✓	0	0	3
GNLY	Tier 3B	✓		✗		✓		✗	✓	0	0	3
NMB	Tier 3B	✓		✓					✓	0	0	3
C1RL	Tier 3B		✓		✗		✗	✓	✓	0	0	3
CYP2D6	Tier 1			✓						321	18	2
NOS3	Tier 1	✓		✓						17	2	2
MAPK3	Tier 1			✗			✓		✗	8	2	2
GDF15	Tier 3A			✓				✗	✗	5	2	2
ITGAM	Tier 3A	✓		✓						9	1	2
TNFRSF10A	Tier 1	✓		✓						1	1	2
TUBB	Tier 1	✓		✓						23	0	2
TG	Tier 3A	✓		✗					✓	14	0	2
RRM1	Tier 1	✓		✗				✗	✓	9	0	2
MPL	Tier 1	✓		✓					✗	8	0	2
CA4	Tier 1	✓		✗				✓	✗	7	0	2
NPPA	Tier 1	✓		✗					✓	2	0	2
ALPL	Tier 2		✓		✓				✗	2	0	2
CDC25B	Tier 2	✓		✗			✓		✗	0	0	2
CAPNS1	Tier 2	✓		✗					✓	0	0	2
MMP24	Tier 3A	✓		✓						0	0	2
TNFSF13	Tier 3A	✓		✓						0	0	2
A2ML1	Tier 3A	✓		✗					✓	0	0	2
INSL3	Tier 3A	✓		✓					✗	0	0	2
HSD3B7	Tier 3B	✓		✓						0	0	2
FZD3	Tier 3B	✓		✓						0	0	2
KLHL24	Tier 3B	✓		✓						0	0	2
BMP8B	Tier 3B	✓		✓					✗	0	0	2
CELSR2	Tier 3B	✓		✓						0	0	2
MUC4	Tier 3B	✓		✓						0	0	2
MLKL	Tier 3B	✓		✓						0	0	2
CNP	Tier 3B	✓		✗			✓		✗	0	0	2
TSPEAR	Tier 3B	✓		✓					✗	0	0	2
SDR42E1	Tier 3B	✓		✓						0	0	2
CD163	Tier 3B		✓		✗			✗	✓	0	0	2
FYN	Tier 1	✓		✗				✗		10	1	1
PRKCD	Tier 1	✓		✗						10	1	1
ITGAL	Tier 1	✓		✗					✗	8	1	1
GPR35	Tier 1	✓		✗						3	1	1

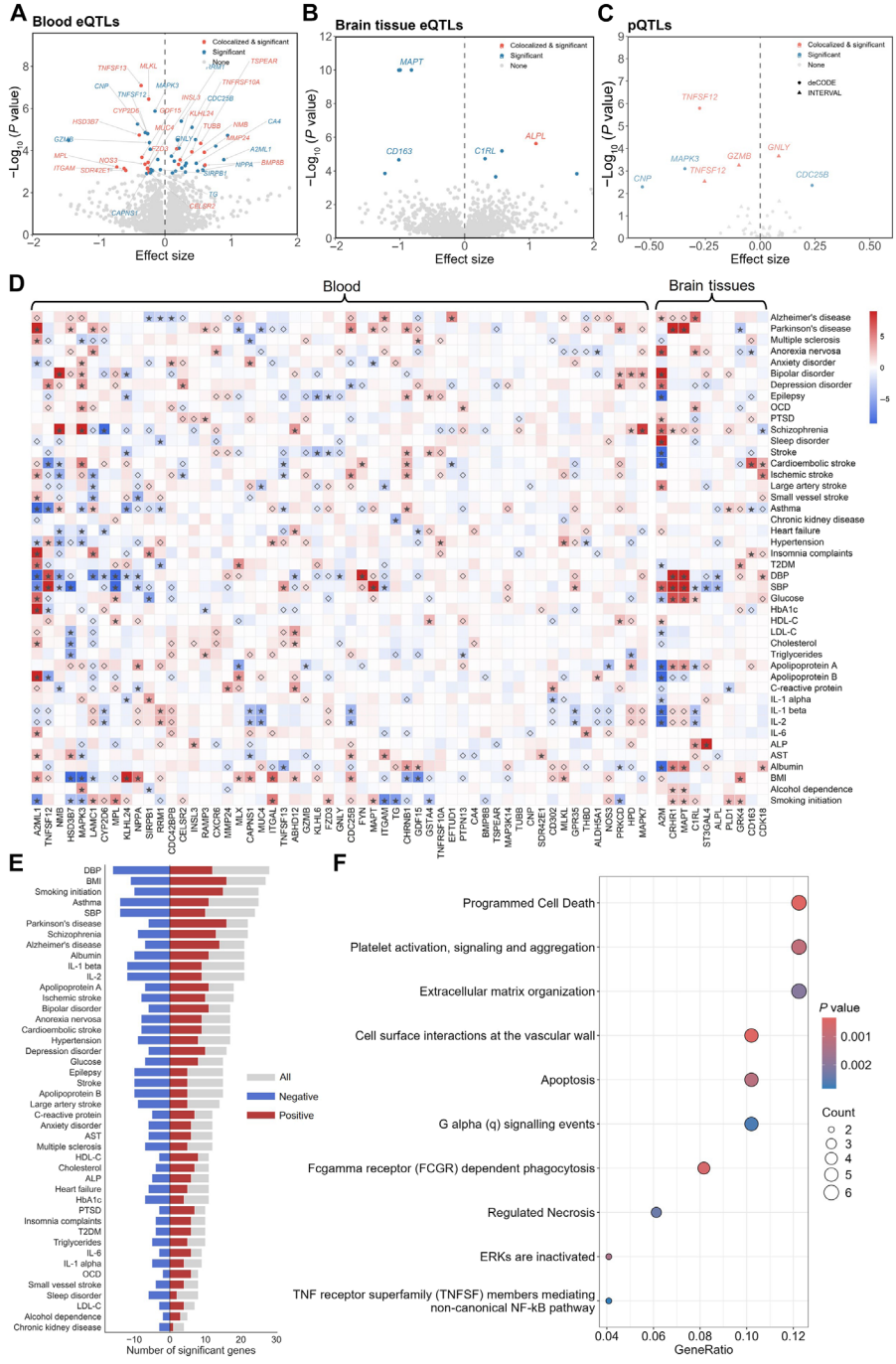

Fig. 4. *Cis*-MR of genes and proteins on BAG. (**A** and **B**) *Cis*-MR of gene expression and colocalization on BAG by tissue-specific eQTLs. (**C**) MR and colocalization of the BAG-associated genes on BAG by plasma pQTLs in INTERVAL and deCODE studies. The *x* axis represents the MR effect per unit (in SD) change (beta) in gene expression or protein level, and the *y* axis represents the $-\log_{10}(P \text{ value})$. Genes are colored and annotated in blue if they pass FDR-corrected *P* value < 0.05 or in red if they are colocalized simultaneously. Genes labeled indicate that they have at least two pieces of evidence in the xQTL analyses. *P* values are truncated at 1×10^{-10} for display purposes. (**D**) Phenome-wide scan of BAG-associated druggable genes. Genes (*x* axis) are categorized and clustered according to tissue types of eQTLs. The 44 phenotypes were categorized and organized into the following groups: neurodegenerative diseases, psychiatric disorders, cerebrovascular diseases, common diseases, biomarkers, and lifestyle factors. Results with a *P* value below the nominal threshold ($P < 0.05$) are indicated by open diamonds, whereas stars indicate *P* values that passed FDR correction (FDR $P < 0.05$). Results are gradient colored based on the direction of the MR effect multiplied by $-\log_{10}(P \text{ value})$. (**E**) The number of BAG-associated genes affected the 44 phenotypes sin the phenome-wide scan. Gray bars indicate total gene counts affecting each phenotype, red bars show positive correlations, and blue bars show negative correlations. (**F**) Reactome pathway enrichment of MR-associated genes. These top 10 significantly enriched pathways are shown (*P* value < 0.05). Abbreviation: ALP, alkaline phosphatase; AST, aspartate aminotransferase; BMI, body mass index; SBP/DBP, systolic/diastolic blood pressure; HbA1c, glycated hemoglobin; HDL-C/LDL-C, high-density/low-density lipoprotein cholesterol; IL-1α/IL-1β, interleukin-1α/β; IL-2/IL-6, interleukin-2/6; OCD, obsessive-compulsive disorder; PTSD, post-traumatic stress disorder; T2DM, type 2 diabetes.

plasma pQTL studies: the INTERVAL study and the deCODE study. As a result, we obtained pQTL data for a total of 35 genes (*GSTA4*, *MAPT*, *TSPEAR*, *BMP8B*, *A2ML1*, *NPPA*, *MAPK3*, *GDF15*, *A2M*, *ITGAL*, *GZMB*, *CNP*, *ALPL*, *ABHD12*, *CDC25B*, *MPL*, *CA4*, *ALDH5A1*, *GNLY*, *INSL3*, *TNFRSF10A*, *PTPN13*, *SIRPB1*, *RAMP3*, *HPD*, *NMB*, *C1RL*, *CAPNS1*, *CD163*, *MUC4*, *RRM1*, *TNFSF12*, *TG*, *CDC42BPB*, and *FYN*). Following MR analysis on pQTLs, we observed that six proteins, granulysin (coded by *GNLY*, beta = 0.08, SE = 0.023, FDR-corrected $P = 0.0030$), granzyme B (coded by *GZMB*, beta = −0.097, SE = 0.028, FDR-corrected $P = 0.0039$), MPIP2 (coded by *CDC25B*, beta = 0.24, SE = 0.083, FDR-corrected $P = 0.041$), ERK-1 (coded by *MAPK3*, beta = −0.34, SE = 0.10, FDR-corrected $P = 0.013$), CN37 (coded by *CNP*, beta = −0.54, SE = 0.19, FDR-corrected $P = 0.041$), and TNF12, exhibited a significant causal effect on BAG (Fig. 4C and data S18). Notably, TNF12, coded by *TNFSF12*, showed consistently significant causal effects on BAG in both INTERVAL study and the deCODE studies (beta = −0.25, SE = 0.085, FDR-corrected $P = 0.013$ in INTERVAL and beta = −0.28, SE = 0.058, FDR-corrected $P = 0.0001$; Fig. 4C and data S18). Furthermore, 14 proteins (gene symbols: *MAPT*, *TNFSF12*, *GZMB*, *SIRPB1*, *GNLY*, *NMB*, *C1RL*, *TG*, *RRM1*, *CA4*, *NPPA*, *CAPNS1*, *A2ML1*, and *CD163*) displayed strong evidence of colocalization. Among them, *C1RL* and *SIRPB1* demonstrated significance in the colocalization analysis using both the deCODE and INTRVAL pQTLs.

Prioritized druggable genes with strong genetic evidence for BAG

Of the 64 druggable genes identified, 37 genes have been supported by at least two pieces of evidence in the MR and colocalization analysis, using the results of BAG GWAS, blood/brain tissue eQTL, and plasma pQTL (Table 1 and table S4). Among these, we have further prioritized seven druggable genes that exhibit at least three pieces of evidence (Table 1), namely, *MAPT*, *TNFSF12*, *GZMB*, *SIRPB1*, *GNLY*, *NMB*, and *C1RL* (Table 1). It is noteworthy that *MAPT* and *TNFSF12* are Tier 1 druggable genes, respectively. This strong evidence in the MR and colocalization analysis with xQTLs suggests that they may serve as promising candidate targets for brain aging.

Phenome-wide scan extends phenotypic associations of the identified targets

We conducted a comprehensive phenome-wide scan using *cis*-MR to investigate the potential effects of the 64 identified druggable genes on 44 traits, with the aim of exploring potential opportunities for drug development (Fig. 4D and data S21). Our analysis revealed frequent associations between these genes and various phenotypes, including diastolic blood pressure (DBP), BMI, smoking initiation, asthma, systolic blood pressure (SBP), PD, SCZ, AD, and albumin levels (Fig. 4E). Specifically, we found that high expression of *MAPT* and *CRHR1* was associated with elevated glucose levels, SBP, DBP, albumin levels, and apolipoprotein A levels and an increased risk of PD. Moreover, high expression of *MPL* was significantly associated with lower SBP and DBP. *SIRPB1*, when expressed at high levels, showed significant associations with insomnia complaints, higher interleukin-1α (IL-1α) and lower glucose levels. Similarly, high expression of *C1RL* was significantly associated with increased risk of OCD, AD, anorexia nervosa, and elevated AST levels while showing lower levels of IL-1β and IL-2. High expression of *A2ML1* demonstrated positive associations with glucose, HbA1c, apolipoprotein B, IL-6, cholesterol, aspartate aminotransferase (AST), BMI, type 2 diabetes (T2DM), MS, PD, small vessel stroke, and ischemic stroke. Conversely, it showed negative associations with SBP, DBP, hypertension, and asthma.

Drug repurposing reveals 29 candidate drugs for brain aging

Our analysis of MR and colocalization has identified 64 druggable genes as potential targets for BAG, suggesting their possible roles in anti-brain-aging mechanisms. By using the drug-gene interaction database, DGIdb, we have identified 466 drugs that are either approved or undergoing clinical development, targeting 29 of the 64 identified genes (Fig. 5A and data S22). Notably, 29 drugs (cholecalciferol, diclofenac, didanosine, doconexent, enalapril, esomeprazole, estradiol, fisetin, glycine, hydrocortisone, ibuprofen, indomethacin, ketoprofen, ketorolac, mecamylamine, mefenamic acid, methylene blue, naproxen, nicotine, piroxicam, prasterone, quercetin, resveratrol, sirolimus, stavudine, sulindac, testosterone, dasatinib, and zidovudine) have shown potential in clinical trials for brain aging, as recorded in ChEMBL or reported by researchers (Figs. 1 and 5B). Among these drugs, 20 (dasatinib, diclofenac, didanosine, enalapril, esomeprazole, fisetin, glycine, ibuprofen, indomethacin, ketoprofen, ketorolac, mefenamic acid, methylene blue, naproxen, piroxicam, quercetin, sirolimus, stavudine, sulindac, and zidovudine) are considered potential geroprotectors, as reviewed by Partridge *et al.* (*32*) and Kulkarni *et al.* (*33*). Thirteen of these drugs (cholecalciferol, dasatinib, diclofenac, doconexent, estradiol, hydrocortisone, mecamylamine, nicotine, prasterone, quercetin, resveratrol, sirolimus, and testosterone) are associated with clinical trials for aging-related indications, as reported in the ChEMBL database.

In the context of brain aging, the prioritization of drug candidates can be based on strong genetic evidence targeting druggable genes. In this study, we have identified a total of 432 drugs that target 15 genes, each supported by at least two pieces of genetic evidence (Table 1 and data S22). Among these drugs, 28 of them, targeting *CA4*, *MPL*, *TUBB*, and *RRM1*, exhibit modes of action that align with the expected direction of the BAG-delaying effect of the targets (Fig. 5B). Specifically, we found that four drugs act as agonists of MPL, whereas 6, 6, and 12 drugs function as inhibitors of *CA4*, *RRM1*, and *TUBB*, respectively (Fig. 5B and data S22). We argue that these 28 drugs hold substantial promise for brain aging.

DISCUSSION

We computationally identify druggable targets for brain aging using a large-scale genetic and imaging data. By leveraging a substantial amount of T1-MRI data, genome-wide genotypes of individuals from UKB, publicly available GWAS datasets of common brain disorders, and xQTLs of druggable genes, this study proposed robust models to estimate the brain age, validate BAG as a heritable trait and a promising biomarker of brain health, and thereafter systematically prioritize potential drug targets for preventing or slowing down brain aging.

A promising finding in our study was the clear advantage of using a state-of-the-art deep learning model, namely, 3D-ViT, for brain age estimation. First, our model demonstrated comparable performance through fivefold cross validation using the training MRI data of 29,097 participants without any brain disorders, suggesting that deep learning models have the potential to effectively characterize aging-related brain changes. Second, our model maintained its performance

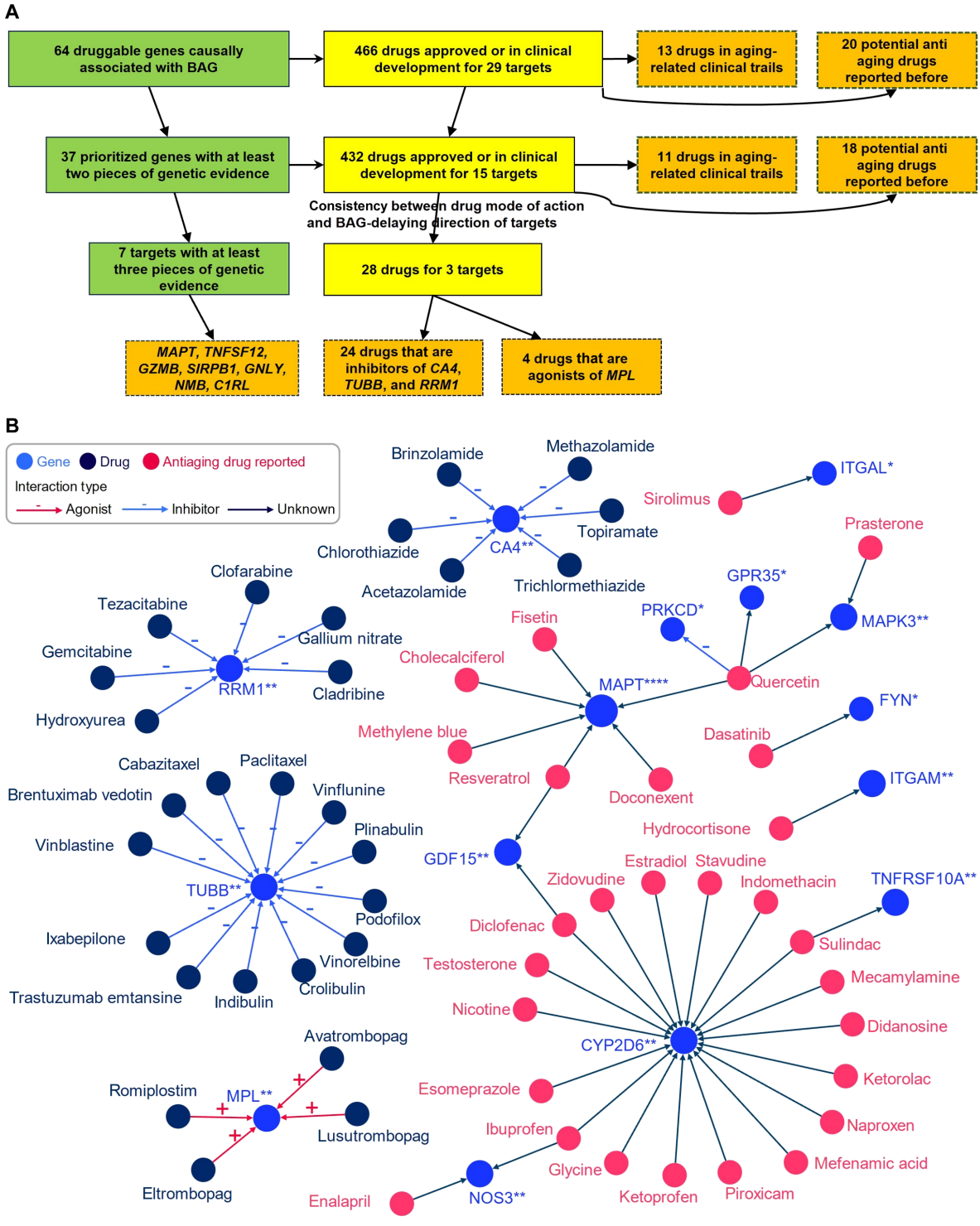

Fig. 5. Drug repurposing for the BAG-associated drugs. (**A**) Pipeline of drug repurposing for brain aging using the druggable genes. Targets and repurposed drugs are prioritized based on the number of the pieces of genetic evidence and the expected effect direction of mode of action. (**B**) Network of the BAG-associated targets and candidate repositioned drugs for BAG. Druggable genes (blue dots) in Table 1, candidate repositioned drugs (dark blue dots), and reported antiaging drugs (red dots) are connected (arrow) based on the drug-gene interaction information queried from DGIdb. The interaction types between drugs and targets are annotated as agonist (blue arrow), antagonist/inhibitor/inverse agonist (red arrow), or unknown (gray arrow). The number of the star symbol "*" after the gene names corresponds to the number of pieces of evidence. For more detailed information on all identified targets and their associated drugs, please refer to data S22.

on an independent testing dataset from UKB and three external independent testing datasets with fine-tuning, demonstrating the high quality of the embedding features learned by the model and its remarkable generalization capability. Third, we observed significantly higher BAG values in subjects with brain disorders compared to the healthy group, which aligns with existing knowledge. Fourth, model interpretation via the saliency map revealed that different subregions of the brain contributed differently to capturing variations related to BAG characterization. It also verified the important roles played by the lentiform nucleus and posterior limb of internal capsule regions in brain aging (*48*–*50*), suggesting the reliable extraction of brain aging-related imaging features. The learned brain imaging features may reflect aging-related microstructural alternations in the brain regions, such as neuronal loss (*51*), blood-brain barrier disruption (*52*), which could be a result of pathophysiological changes, and the different weights assigned to subregions might further demonstrate their different role in these changes. Last, several genomic loci identified by the GWASs for binary groups of BAG replicated previous findings from GWAS for continuous values of BAG, including *CRHR1* and *RUNX2* (*4*, *17*). These findings reinforce the validity of the proposed deep learning model.

A previous study has indicated that BAG is a heritable and polygenic trait with genetic associations to common brain disorders (*25*). BAG has also been reported in cognitive studies, independent of patients with neurodegeneration and neuropsychic disorders, suggesting that it is an essential marker of cognition function (*4*). In addition to confirming the associations between well-known genes like *RUNX2*, *CRHR1*, and *INPP5A* with BAG (*4*), our study has also identified genes, including *TP53*, that are associated with BAG in the context of brain aging. Particularly, the phenotypes of accelerated aging mice, showing chronic p53 activation, could be rescued upon p53 deficiency (*45*), indicating its functional association with brain aging. However, further investigation is needed to fully understand the detailed relationship between these factors.

An intriguing question that needs to be addressed is whether brain disorders and brain aging have causal effects and, if so, in which direction. To accurately identify druggable targets for brain aging, it is crucial to mitigate the confounding impact of brain disorders on brain aging. In a related study, Leonardsen *et al.* (*4*) investigated the causal relationships between BAG and five brain disorders, namely, PD, AD, MDD, SCZ, and BIP. They discovered a nominally significant causal influence of AD and BIP on BAG. Kaufmann *et al.* (*25*) also found that BAG is increased in several common brain disorders, but they have overall weak correlations. Moreover, they argued that BAG and brain disorders partly shared molecular genetic mechanisms. In this study, we examined the causal relations between 18 common brain disorders and BAG and found that these causal relations were not statistically significant after applying multiple-testing correction. One possible interpretation for the weak associations is the inherent heterogeneity of brain disorders and brain aging. Yang *et al.* (*53*) identified brain aging heterogeneity with five dominant patterns of brain atrophy. Conditions such as AD, PD, and MDD exhibit diverse subtypes with distinct pathologies, genetic architectures, and clinical characteristics (*54*–*57*), which could weaken any shared associations with BAG. Thus, a more stringent sample selection might be required to detect the causal associations between BAG and brain disorders. On the other hand, the overall weak associations may also suggest that BAG reflects a more comprehensive digital phenotype of brain aging rather than serving as a pathological biomarker for a specific disorder. Nonetheless, individuals with brain disorders exhibited higher BAG values compared to healthy participants, indicating that the causal relations of various brain disorders on BAG should be carefully tackled.

To efficiently identify potential drug targets for individuals without brain disorders but at high risk for rapid brain aging, we conducted a GWAS using participants from UKB who did not have any brain disorders. This allowed us to eliminate confounding factors such as changes in the brain caused by brain disorders, which could potentially contribute to abnormal aging. The GWAS analysis could pinpoint the BAG-associated loci but with unclear causal relationship. Therefore, we genetically prioritized druggable genes that could potentially slow down brain aging by using *cis*-MR and colocalization approaches, along with GWAS of BAGs and xQTL data. Both blood and brain tissue eQTLs were incorporated in this study to encompass a wide range of genes. We present an approach to transition from genetically supported signals of BAG to identifying drug targets of brain aging. Among the identified drugged or druggable genes (Table 1), we emphasize the promising potential of seven specific genes, namely, *MAPT*, *TNFSF12*, *GZMB*, *SIRPB1*, *C1RL*, *NMB*, and *GNLY*. These genes are supported by at least three pieces of genetic evidence, suggesting their potential as viable drug targets for brain aging.

Targets with more causal genetic evidence support may be prioritized. *MAPT* exhibits a negative and causal association with BAG in both blood and brain tissues (beta = −2.27 and −0.82, respectively). In addition, the expression of *MAPT* at both transcript and protein levels is colocalized with BAG (PPH4 = 1 and 0.93, respectively). However, these causal associations are supported by only one SNP in blood and brain, respectively, indicating weak reliability due to the presence of weak instruments. Meanwhile, higher levels of *MAPT* are positively associated with elevated glucose levels, SBP, DBP, and apolipoprotein A and an increased risk of PD. Although it has been suggested that reducing tau may alleviate the pathology of AD (*51*), the role of *MAPT* in the interaction between brain aging and certain brain disorders appears complex (*51*). Collectively, further investigation of the role of *MAPT* in brain aging is warranted. *TNFSF12*, supported by four pieces of genetic evidence, demonstrates a negative and causal association with BAG at both the transcript and protein levels. This association is observed in both the deCODE and INTRVAL pQTL datasets. Furthermore, TNF12, a cytokine belonging to the tumor necrosis factor (TNF) ligand family, is colocalized with BAG. TNF12 (also known as TWEAK) plays an important role in blood-brain barrier inflammation (*58*) and has a protective effect on glucose homeostasis (*59*), both of which are highly involved in brain aging (*48*). Meanwhile, *GNLY*, *GZMB*, *SIRPB1*, *NMB*, and *C1RL*, with three pieces of genetic evidence in the post-GWAS analysis, show promising in delaying brain aging. The expression of *GNLY* is positively and causally associated with BAG at both transcript and proteomic levels, and granulysin (encoded by *GNLY*) is colocalized with BAG (PPH4 = 1). Granulysin is an antimicrobial and proinflammatory peptide in the granules of human cytotoxic T lymphocytes and natural killer cells and could activate expression of C-C Motif Chemokine Ligand 5 (CCL5), Monocyte chemoattractant protein-1 (MCP-1), IL-10, IL-1β, IL-6, and IFN-α (interferon-α) (*60*). Similarly, the expression of *GZMB* is negatively and causally associated with BAG at both transcript and proteomic levels, and its protein, granzyme B, is colocalized with BAG (PPH4 = 1). Granzyme B, a serine protease, is known to mediate the

secretion of IL-8 and Macrophage inflammatory protein 2 (MIP2) (*61*) and has been implicated in skin aging and vascular wall inflammation (*62*, *63*). Given that inflammation is an endogenous factor in aging, targeting such pathways could be a potential antiaging strategy (*64*). Furthermore, *SIRPB1* demonstrates a causal association (beta = −0.07) with BAG, and the abundance of SIRB1 (encoded by *SIRPB1*) is colocalized (PPH4 = 0.92) with BAG. *SIRPB1*, belonging to the immunoglobulin superfamily, has shown significant correlation in centenarian-based longevity genetic studies (*65*). *NMB*, a neuropeptide, is positively and causally associated with BAG. Notably, *NMB* is associated with eating behaviors and obesity (*66*), which are important factors in aging (*67*). *C1RL*, a positively causal target for BAG in brain tissue, is colocalized with BAG within both deCODE and INTRVAL pQTL datasets (PPH4s = 1), and is associated with AD in the phenome-wide association study (PheWAS) result. Notably, *C1RL* is primarily involved in biological processes related to the immune response and has been shown to activate genes encoding transcription factors related to crucial cellular processes and inflammation (*68*). Given the association of these genes with cellular processes and inflammation, which likely contribute to neuropathogenesis and subsequent brain aging (*69*, *70*), *TNFSF12*, *GNLY*, *GZMB*, *SIRPB1*, *NMB*, and *C1RL* are prioritized targets for brain aging.

Several genes with two pieces of genetic evidence in the MR and colocalization analysis have shown promise as drug targets for brain aging. For instance, *MPL* encodes a protein similar to members of the hematopoietic receptor superfamily. Mutations in *MPL* can lead to thrombocytosis, resulting in abnormal *MPL* trafficking or receptor activation (*71*). *MPL* is negatively and significantly associated with BAG (beta = −0.72) in the MR using blood eQTL data and colocalized with BAG (PPH4 = 1), suggesting that higher expression of *MPL* is causally associated with a younger brain age. Higher expression of *MPL* is significantly associated with lower SBP and DBP. Notably, cumulative blood pressure is associated with subsequent cognitive decline and dementia risk, suggesting that controlling blood pressure could be beneficial for both neurocognition and longevity (*72*, *73*). These findings indicate that further investigation is warranted to understand how mutations in *MPL* are associated with brain aging. *ALPL* is also a promising target, as it is causally associated (beta = 1.1) and colocalized (PPH4 = 0.76) with BAG in brain tissue. *ALPL* is an age–up-regulated phosphatase, and inhibiting *ALPL* can enhance transcytosis of plasma (*74*). Increased levels of *ALPL* in plasma are anticorrelated with cognitive performance (*75*). *TUBB*, a structural component of microtubules, is another MR target gene and colocalized with BAG (PPH4 = 0.96). *TUBB* is associated with cortical dysplasia, microcephaly, and developmental delay (*76*). *RRM1*, belonging to ribonucleotide reductase, is positively and causally associated (beta = 0.40) with BAG, and its protein is colocalized with BAG (PPH4 = 1). Recently, *RRM1* has been found to be causally associated with telomere length, a hallmark of biological aging (*77*). *CA4*, positively and causally associated with BAG, is a zinc metalloenzyme and involved in blood-brain barrier crossing (*78*). The relations between the other MR genes and aging are described in the Supplementary Text. Collectively, we have identified several candidate targets for brain aging, supported by genetic evidence and the literature. Further research is needed to elucidate how these genes are involved in the aging process and to evaluate their potential as therapeutic targets.

To provide a comprehensive genetic profile and explore potential repurposing opportunities for the identified drug targets, we conducted a PheWAS analyzing variants within and around these targets across 44 traits. PheWAS, serving as a valuable tool for drug discovery, confirmed several previously known causal associations or biological pathways related to specific clinical traits. For instance, it revealed associations between *GDF15* and BMI (*79*), as well as *MAPT* and neurodegenerative disorders (*80*). Nevertheless, further investigations are needed to assess the causal relationship between each target and the corresponding trait, as well as to evaluate the potential beneficial or detrimental effects of modulating these targets for the prevention of brain aging from a pharmacological perspective.

Drug repurposing for the genetically supported druggable genes results in the rediscovery of 29 drugs, which are either in clinical trials for aging or have been previously reported as potential antiaging drugs, indicating the power of our pipeline and highlights its effectiveness. The strategy of drug repurposing substantially improves the success rate and reduces the likelihood of side effects associated with repurposed drugs for drug development. For instance, stavudine (targeting *CYP2D6*), a LINE1 reverse-transcriptase inhibitor, could rescue the young inflammation profile in mice and lower about 30% DNA methylation age, significantly improved health and life span of *SIRT6* knockout mice (*81*). Sirolimus, also known as rapamycin, inhibits mTOR pathway and promotes health and longevity in diverse model organisms. It has beneficial effects on aging human organ systems, especially the brain and immune system (*82*, *83*). Sirolimus is involved in several ongoing aging-related clinical trials, such as resetting the epigenetic clock (NCT04608448), ovarian aging (NCT05836025), and preventing functional decline in older adults (NCT05237687). Therefore, our findings suggest that other drugs in our results may be repurposed to delay brain aging, and ongoing aging-related clinical trials of the rediscovered drugs further support this notion.

Moreover, among the 37 druggable genes supported by at least two pieces of genetic evidence, we have identified 28 drugs targeting *MPL*, *CA4*, *TUBB*, and *RRM1*, although neither in clinical trials nor reported previously have the potential to be repurposed for slowing down brain aging. Specifically, four drugs, namely, avatrombopag, eltrombopag, lusutrombopag, and romiplostim, which are typically used for thrombocytopenia, act as agonists for *MPL*. As mentioned above, *MPL* is a thrombopoietin receptor and has been linked to platelet count and brain morphology in the GWAS catalog. Notably, platelet signaling and aggregation pathway is enriched using the 64 MR genes. It is worth noting that platelet count decreases during aging and is lower in men compared to women (*84*). A recent study of platelets has also revealed that platelets rejuvenate the aging brain (*85*). Schroer *et al.* (*86*) found that circulating platelet-derived factors could potentially serve as therapeutic targets to attenuate neuroinflammation and improve cognition in aging mice (*86*). Park *et al.* (*87*) reported that longevity factor klotho induces multiple platelet factors in plasma, enhancing cognition in the young brain and decreasing cognitive deficits in the aging brain (*87*). Leiter *et al.* (*88*) found that platelet-derived platelet factor 4, highly abundant chemokine in platelets, ameliorates hippocampal neurogenesis, and restores cognitive function in aged mice. These findings suggest that the aforementioned drugs may enhance the expression of *MPL*, leading to increased platelet count and potentially contributing to a delay in brain aging. It is important to note that determining the significant tissue(s) for gene prioritization can be challenging. Although brain tissues may be more biologically relevant for brain

aging, circulating proteins have the capability to modulate brain aging as well (*89*, *90*). Six drugs (cladribine, clofarabine, gallium nitrate, gemcitabine, hydroxyurea, and tezacitabine) are inhibitors of *RRM1*, whereas 12 drugs (brentuximab vedotin, cabazitaxel, crolibulin, indibulin, ixabepilone, paclitaxel, plinabulin, podofilox, trastuzumab emtansine, vinblastine, vinflunine, and vinorelbine) are inhibitors of *TUBB*. Most of these drugs targeting *RRM1* and *TUBB* are antineoplastic agents used in cancer treatment. In addition, six drugs (acetazolamide, brinzolamide, chlorothiazide, methazolamide, topiramate, and trichlormethiazide) are inhibitors of *CA4* and most of them are used for hypertension.

There are a few limitations to this study: (i) The accurate estimation of brain age is hindered by the lack of ground-truth brain biological age and discrepancies between brain biological age and chronological age in supposedly healthy individuals. The estimated brain age derived from MRI data includes inherent biases (*91*). Although our model has shown better generalization performance compared to other models, there is always an expectation for a more accurate brain age estimation model that can deliver more robust outcomes for clinical applicants (*3*, *91*). (ii) Potential data bias may affect the findings of this comprehensive study. For instance, the brain age estimation model and GWAS summary statistics primarily relied on cohorts of European white individuals, potentially overlooking druggable targets that would be effective in individuals of non-European ancestry. Validation using genomic and clinical data from more diverse populations could help remedy this limitation. (iii) Validation on independent discovery and replication cohorts would enhance the reliability of the identified genes as drug targets for the prevention of brain aging. Although we maximized statistical power using the UKB data as a large discovery cohort, the absence of a discovery-replication design is unavoidable. As large-scale datasets containing both MRI and genome-wide genotypes were not widely available, we used a combination of GWAS for BAG, MR with xQTL, colocalization analysis, MR-PheWAS, and the existing literature to carefully identify genetic targets that are supported by evidence for their involvement in brain aging. With the availability of more comprehensive proteomics platforms and the inclusion of more diverse non-European ancestry populations in studies, it is likely to replicate and validate our results. (iv) Brain aging is a complex process involving numerous potential causes, such as aging of cerebral blood vessels (*92*), atrophy of the cerebral cortex (*93*), etc. These causes may overlap and interweave, undergoing considerable changes during brain aging (*48*). Although our study demonstrates the utility of systematically analyzing GWAS alongside extensive brain imaging information and xQTL analysis to enrich the identification of drug targets, there remains a need for machine learning or statistical methods to address the various risk factors associated with brain aging. Fine-grained analysis is a must to comprehend the individualized causes and trajectories of brain aging, enabling the identification of effective drug targets and the use of precision medications for the purpose of slowing down or even preventing brain aging. There is also an increasing need for comprehensive studies spanning different tissues and organs to evaluate tissue- or organ-specific effects of targets, enabling the systematic prevention or treatment of human aging. (v) This study did not explore adverse effects of the rediscovered antiaging drugs. This is particularly important because healthy aging individuals should be encouraged to consider the potential risks associated with taking medications or supplements for slowing down aging as these interventions may have unintended negative consequences for both individuals and society. Alternatively, it is worthwhile to explore nonpharmacological interventions/digital therapies that can help preserve mental and physical fitness in people during aging.

In summary, we present a systematic study for identify genetically supported targets and drugs for brain aging with deep learning-based brain age estimation, GWAS for BAG, analysis of the relation between BAG and brain disorders, prioritization of targets using MR and colorization analysis for BAG with xQTL data, drug repurposing for these targets of BAG, and PheWAS. Our results offer the potential to mitigate the risk associated with drug discovery by identifying genetically supported targets and repurposing approved drugs to attenuate brain aging. We anticipate that our findings will serve as a valuable resource for prioritizing drug development efforts for BAG, shedding light on the understanding of human brain aging and potentially extending the health span in humans.

MATERIALS AND METHODS

MRI datasets

We trained and evaluated our brain age estimation model using T1-weighted MRI data from UKB (application number 89757). The UKB dataset consists of 42,904 subjects with T1-weighted MRI data, ranging in age from 45 to 82 years old. To account for potential population structure bias, we limited our analysis to 38,961 subjects of White British ancestry (Fig. 1A). Within this restricted dataset, there were 32,324 subjects without brain disorders, including 6036 healthy individuals and 26,288 subjects without any brain disorders. In addition, there were 6637 subjects recorded with brain injury, neurodegeneration, or neuropsychiatric disorders.

To externally validate the performance and generalizability of our brain age estimation model, we used three other datasets: the ADNI dataset (https://adni.loni.usc.edu/), the PPMI dataset (https://ppmi-info.org/), and the IXI dataset (https://brain-development.org/ixi-dataset/). The ADNI dataset is a longitudinal multicenter study that includes participants categorized as cognitively normal (CN), mild cognitive impairment (MCI), and those with AD. We selected 1627 CN subjects from the ADNI datasets, ranging in age from 60 to 96 years old. The PPMI dataset comprises subjects with PD at various stages, from prodromal to moderate disease, enrolled at ~50 sites. This dataset provides comprehensive longitudinal data on clinical features and MRI outcomes. We specifically extracted T1-weighted MRI scans from 259 healthy participants aged between 45 and 83 years old. The IXI dataset consists of nearly 600 MRI images from normal and healthy participants of various ages collected across three hospitals in London. From this dataset, we extracted 313 healthy participants aged between 45 and 84 years old.

MRI data preprocessing

For the UKB dataset, we used T1-weighted data that had already been registered to the Montreal Neurological Institute 152 (MNI152) standard space. As for the validation datasets (IXI, ADNI, and PPMI), we preprocessed the T1-weighted MRI data using a minimal preprocessing scheme with tools from FSL (*94*, *95*) (FMRIB Software, version 6.0.5, https://fsl.fmrib.ox.ac.uk/fsl/fslwiki/). First, we reoriented the generated volume of the raw MRI images to match the standard direction in FSL. Second, we cropped the MRI images, removing the neck and everything below the head region. In addition, we performed bias field correction (without segmentation) and

eliminated non-brain tissue from the entire head images. Last, we applied linear and nonlinear registration techniques with 6 degrees of freedom to align the MRI images with the standard MNI152 template. All preprocessed MRI volumes had a voxel size of $182 \times 218 \times 182$ and maintained an isotropic spatial resolution of 1 mm^3.

Brain age estimation

We trained seven state-of-the-art deep learning models (*96*), namely, ResNet, VGGNet, EfficientNet, SFCN, DenseNet, GLT, and 3D-ViT model for brain age estimation (Fig. 1A). A systematic comparison of these six deep learning models for brain age estimation using MRI samples from the UKB demonstrates that 3D-ViT outperformed the other models. Hence, we chose 3D-ViT for brain age estimation in the subsequent analyses. Briefly, we first resized T1 weighted MRI images to a resolution of $128 \times 128 \times 128$ as input to the model. We used the multihead attention mechanism of the 3D-ViT to divide the original MRI image into a set of 3D patches (patch size: $16 \times 16 \times 16$). These patches were processed through a transformer encoder, which measured attention scores between them. A multilayer perceptron header was then used to summarize the outputs from the transformer encoder for brain age estimation.

We implemented 3D-ViT for brain age estimation (Fig. 2A) using PyTorch (version 1.13.1, CUDA version 8.6). The model was trained on 90% (29,097 of 32,324 subjects) of the subjects without brain disorders. The training data was adjusted by sex and site effect. The remaining 9864 subjects (including 3227 non-brain disorder subjects) were reserved for testing. We used a fivefold cross-validation strategy to train the model. The training data was randomly divided into five folds, with four folds used for training and the remaining fold for evaluation. This process was repeated five times, resulting in brain age estimation for all training subjects. Subsequently, the trained model was used to estimate brain age on the testing dataset and three external datasets: ADNI, PPMI, and IXI. The model's performance was evaluated using MAE, MSE, R^2, and r between the estimated brain age and chronological age. The model was optimized using the Adam optimizer with 200 epochs and a learning rate of 2.0×10^{-5}. We performed early stopping to prevent potential overfitting problems if the validation error did not improve within 10 epochs.

Interpretation of brain age estimation with saliency maps

Saliency maps were computed for the used 3D-ViT model by calculating the gradients on the test data. Specifically, the MSE loss was computed between the estimated brain age and the chronological age, and then backpropagation was used to determine the gradient of this loss with respect to the input MRI images. Then, the saliency value of each voxel was obtained by taking the absolute value of the gradient, which represents the magnitude of influence of that voxel on the model's prediction. Subsequently, these saliency maps were normalized to generate saliency probability maps, thereby providing a probabilistic interpretation of voxel-wise significance in age estimation.

GWAS on BAG

We conducted the GWAS analysis using genotyped and imputed data obtained from UKB (GRCh37 assembly) on 31,520 non-brain disorder participants (Fig. 1B). Subjects with brain disorders were not used in the GWASs to avoid the confounding effects from brain disorders. In brief, the samples were genotyped using the Affymetrix BiLEVE and Axiom arrays, and untyped variants were imputed using the Haplotype Reference Consortium, 1000 Genomes, and UK10K as reference panels (*35*). Standard quality control procedures were applied to exclude samples and SNPs that did not meet certain criteria. Samples with a phenotype deletion rate above 0.05, minor allele frequencies below 0.01, and deviations from Hardy-Weinberg equilibrium ($P < 1 \times 10^{-6}$) were removed. For the genetic association analysis, we used Plink software (version 1.90 beta, https://cog-genomics.org/plink/) and assumed an additive genetic model. Covariates including chronological age, sex, and the top 10 principal components were included to account for population stratification, suggested by (*25*, *97*). The standard GWAS significance threshold was set as 5.0×10^{-8}.

In addition to the continuous BAG-based GWAS, we implemented a case-control grouping strategy using a specific threshold value μ of BAG. This allowed us to categorize subjects into two nonoverlap groups for conducting case-control BAG-based GWAS. In particular, we conducted GWASs by comparing of BAG $> \mu$ versus BAG $\leq \mu$, BAG $< -\mu$ versus BAG $\geq -\mu$ ($\mu = 1, 2, 3, 4$, and 5, respectively) and the highest 25% of BAG versus the lowest 25% of BAG. Thereafter, we evaluated the statistical power of each GWAS, by calculating the number of independent genome-wide-significant loci and other relevant statistics. Our results demonstrated that the GWAS using continuous BAG exhibited the highest statistical power among all the GWASs we implemented (table S2). Hence, we chose to use the GWAS results obtained from the continuous BAG for subsequent analyses.

Post-GWAS annotations

We used the web application Functional Mapping and Annotation (FUMA) (*98*) to annotate BAG-associated SNPs and perform gene mapping (Fig. 1B). Independent significant SNPs were identified using the LD reference panel from UKB release 2b 10k White British with the following parameters: P value $= 5 \times 10^{-8}$, $r^2 = 0.6$, and second $r^2 = 0.1$. The standard interregional distance threshold of 250 kb were used, as per the default settings in FUMA (*98*), where SNPs with the smallest association P values were selected as the lead SNPs for the corresponding regions. Genes falling within the boundaries of each region, determined by their genomic coordinates, were assigned to the corresponding region. In addition, we examined the expression levels of the annotated genes linked to the associated SNPs across 54 tissue types using the GTEx v8 dataset.

Genetic correlation between BAG and brain disorders/phenotypic traits

We assessed the genetic correlations between BAG and 18 common brain disorders (Fig. 1C): neurodegenerative disorders (AD, PD, MS, and EP), psychiatric disorders (AN, ANX, BIP, MDD, OCD, PTSD, TS, SCZ, and SLD), and stroke (stroke, ischemic stroke, large artery stroke, cardioembolic stroke, and small vessel stroke). GWAS summary statistics for AD, MS, AN, ANX, BIP, MDD, OCD, PTSD, and SCZ were obtained from the Psychiatric Genomics Consortium (https://med.unc.edu/pgc/download-results). GWAS summary statistics for PD were obtained from the International Parkinson Disease Genomics Consortium (https://gwas.mrcieu.ac.uk/datasets/ieu-b-7/). In addition, GWAS summary statistics for stroke were downloaded from the MEGASTROKE consortium (http://megastroke.org/) (*99*) and GWAS summary statistics for MS, EP, and SLD were downloaded from the FinnGen project (https://finngen.fi), a resource known for its comprehensive genetic data derived from the Finnish population. Data S23 provides detailed population information for each GWAS

summary used in this study. We used LDSC (*28*) to estimate SNP heritability for GWAS summary statistics of BAG and genetic correlations between BAG and the 18 brain disorders. Only high-quality SNPs published in the HapMap3 dataset were used for estimation. The LD score derived from the 1000 Genomes projects phase 3 EUR dataset (1KGp3) was used for LDSC analysis. To correct for multiple testing across all brain disorders, we applied the Benjamini-Hochberg FDR procedure. The statistically significant threshold was set at FDR-corrected $P < 0.05$.

In addition, we assessed the genetic correlations between BAG and eight phenotypic traits (Fig. 1C): alcoholic drinks per week, cigarettes per day, education years, insomnia, intelligence, neuroticism, obesity, and smoking initiation. Specifically, GWAS summary statistics for alcoholic drinks per week, cigarettes per day, and the smoking initiation were sourced from the GSCAN Consortium (GWAS & Sequencing Consortium of Alcohol and Nicotine use; https://gscan.eu/). In addition, GWAS summary statistics for insomnia and obesity were acquired from the FinnGen project (https://finngen.fi). The educational attainment, quantified in terms of years of education, was analyzed based on data provided by Rietveld *et al.* (*100*) from the SSGAC (Social Science Genetic Association Consortium). Furthermore, GWAS summary statistics for neuroticism were obtained from the Genetics of Personality Consortium. Last, GWAS summary statistics for intelligence were sourced from the GWAS catalog (https://ebi.ac.uk/gwas/home). Data S23 provides detailed information of GWAS summaries for these traits.

MR between BAG and brain disorders/phenotypic traits

Bidirectional two-sample MR was conducted to examine the causal relations between BAG and 18 common brain disorders (Fig. 1D) and between BAG and eight phenotypic traits (Fig. 1D). All MR analyses in this study used the R package "TwoSampleMR" (version 0.5.6) with five default methods: inverse variance weighted (IVW), MR-Egger, weighted median, simple mode, and weight Mode. As exposure data, we selected SNPs that surpassed the significance threshold ($P < 5.0 \times 10^{-8}$) as instrument variables for each GWAS summary. These selected SNPs were then clumped at an $r^2 = 0.1$ within a 1000-kb window size, using the LD panel of 1KGp3 to account for LD and minimize interference. *F*-statistic was used to filter out weak instruments, i.e., SNPs with low statistical power (*F*-statistic < 10). Thereafter, the exposure and outcome data were harmonized based on the same effect alleles and palindromic SNPs were removed before conducting the MR analysis. In the MR analysis, an FDR-corrected *P* value less than 0.05 is considered significant, which is also applicable to all the following MR analysis.

MR using *cis*-eQTL analysis

Tissue-specific *cis*-eQTL data were obtained from two consortia: eQTLGen (Blood eQTLs; https://eqtlgen.org/) (*101*) and PsychENCODE (Brain tissue eQTLs; http://resource.psychencode.org/) (*102*). From the eQTLGen consortium, we downloaded full significant *cis*-eQTL results with an FDR-corrected *P* value < 0.05, along with allele frequency information. From the PsychENCODE consortia, we obtained eQTLs (FDR-corrected $P < 0.05$) for genes with expression >0.1 FPKM (fragments per kilobase per million mapped fragments) in at least 10 samples, as well as all SNP information (*103*). Specifically, the obtained eQTL data includes 10,507,664 *cis*-eQTLs for 16,987 genes associated with blood eQTLs and 6,378,784 *cis*-eQTLs for 32,944 genes associated with brain tissue eQTLs.

Thereafter, we used the druggable genome data, containing 4479 druggable genes and obtained from Finan *et al.* (*34*), to filter genes of eQTL and pQTL. First, we removed nonautosomal genes, resulting in 4317 druggable genes. Then, we filtered genes for both eQTL datasets and *cis*-eQTLs within 250-kb upstream or downstream of the target druggable gene. This process yielded 2682 druggable genes specifically associated with blood and 2915 druggable genes associated with brain tissues.

To assess the causal effects of these druggable genes on BAG, we conducted *cis*-MR analysis using the same clumping and harmonizing metrics as the MR analysis between BAG and brain disorders (Fig. 1E). For genes that had only one SNP available, Wald ratios were calculated. In cases where multiple SNPs were present, the IVW method was used for the *cis*-MR analysis. However, it is important to consider the potential bias introduced by genetic variants influencing the outcome through a pathway other than the exposure (i.e., horizontal pleiotropy) (*104*). To address this concern, we performed the MR-Egger intercept test as a sensitivity analysis when three or more SNPs were available. A *P* value greater than 0.05 indicates nonsignificant horizontal pleiotropy. Of note, this strategy is also applied to the following MR analyses. In addition, we used clusterProfiler (*105*) to implement the Reactome pathway enrichment analysis with the MR-identified genes.

Colocalization analysis

The colocalization analysis between the genes identified with MR effects and BAG was conducted using the R package "coloc" to provide additional confirmation that the gene expression and BAG shared the same causal variant within the region of interest (Fig. 1E). This analysis aimed to distinguish whether the variant sharing was coincidental due to correlation through LD or if it indicated a true causal relationship. For each gene tested, we used default priors: $P_1 = 10^{-4}$, $P_2 = 10^{-4}$, and $P_{12} = 10^{-5}$, where P_1, P_2, and P_{12} are the prior probabilities that a SNP in the tested region is significantly associated with the expression of the tested gene and BAG, or both, respectively (*106*). The colocalization yields posterior probabilities associated with five hypotheses: PPH0 (no association with either trait), PPH1 (association with expression of the gene but not with BAG), PPH2 (association with BAG but not expression of the gene), PPH3 (association with the BAG and expression of the gene, with distinct causal variants), and PPH4 (association with BAG and expression of the gene, with a shared causal variant). Following the commonly used setting (*106*), we considered SNPs reaching a posterior probability of PPH4 > 0.75 as colocalized SNPs (*106*).

pQTL analysis

We used pQTL data from two large-scale studies: the INTERVAL study (https://www.ebi.ac.uk/gwas/publications/29875488) (*107*) and the deCODE study (https://decode.com/) (*108*). The INTERVAL study involved the measurement of 3622 proteins in 3301 healthy European blood donors, leading to the identification of 1927 pQTLs for 1478 proteins. The deCODE study conducted GWAS of plasma protein levels using 4907 aptamers in a cohort of 35,559 Icelanders. Specifically, we identified pQTLs available from these two studies for 38 druggable genes associated with BAG among the 64 druggable genes. All pQTLs included in our analysis exhibited FDR-corrected *P* values < 0.05 in their respective original pQTL studies. The MR and colocalization analysis using pQTL are similar to that using eQTL data as described above (Fig. 1F).

Phenome-wide scan for the BAG-associated druggable genes

For genes that were identified with a causal effect on BAG, we evaluated their effects on 44 clinically relevant biomarkers or diseases by combining the *cis*-MR with a phenome-wide scan (Fig. 1G). This allowed us to further investigate the potential druggable genetic effects that could be relevant for future drug development programs. As appropriate, we considered a nominal P value < 0.05 to be significant, and we applied a conservative threshold of FDR-corrected P value < 0.05. Detailed information of the GWAS summary for the 44 clinically relevant biomarkers or diseases is provided in table S5.

Drug repurposing

Drug repurposing for brain aging is implemented using the 64 druggable targets (Fig. 1H). The drug and target information were retrieved from the DGIdb webserver, which stands for the Drug Gene Interaction Database (https://dgidb.org, accessed in June 2023) (*109*). The clinical trial stage of these drugs was obtained from the DrugBank database (https://go.drugbank.com/, version 5.1.8, downloaded in June 2021) (*110*), and the indications of the drugs were downloaded from the ChEMBL database (https://ebi.ac.uk/chembl, version 33, accessed in July 2023) (*31*). The R package "dplyr" was used to query the localized DrugBank and ChEMBL databases.

Supplementary Materials

The PDF file includes:

Supplementary Text
Figs. S1 to S35
Tables S1 to S5
Legends of data S1 to S23
References

Other Supplementary Material for this manuscript includes the following:

Data S1 to S23

REFERENCES AND NOTES

1. Z. D. Zhang, S. Milman, J.-R. Lin, S. Wierbowski, H. Yu, N. Barzilai, V. Gorbunova, W. C. Ladiges, L. J. Niedernhofer, Y. Suh, P. D. Robbins, J. Vijg, Genetics of extreme human longevity to guide drug discovery for healthy ageing. *Nat. Metab.* **2**, 663–672 (2020).
2. D. Goldman, The economic promise of delayed aging. *Cold Spring Harb. Perspect. Med.* **6**, a025072 (2015).
3. M. Tanveer, M. A. Ganaie, I. Beheshti, T. Goel, N. Ahmad, K.-T. Lai, K. Huang, Y.-D. Zhang, J. Del Ser, C.-T. Lin, Deep learning for brain age estimation: A systematic review. *Inf. Fusion* **96**, 130–143 (2023).
4. E. H. Leonardsen, D. Vidal-Piñeiro, J. M. Roe, O. Frei, A. A. Shadrin, O. Iakunchykova, A.-M. G. de Lange, T. Kaufmann, B. Taschler, S. M. Smith, O. A. Andreassen, T. Wolfers, L. T. Westlye, Y. Wang, Genetic architecture of brain age and its causal relations with brain and mental disorders. *Mol. Psychiatry* **28**, 3111–3120 (2023).
5. K. Franke, C. Gaser, Ten years of *BrainAGE* as a neuroimaging biomarker of brain aging: What insights have we gained? *Front. Neurol.* **10**, 789 (2019).
6. J. H. Cole, K. Franke, Predicting age using neuroimaging: Innovative brain ageing biomarkers. *Trends Neurosci.* **40**, 681–690 (2017).
7. S. He, D. Pereira, J. David Perez, R. L. Gollub, S. N. Murphy, S. Prabhu, R. Pienaar, R. L. Robertson, P. Ellen Grant, Y. Ou, Multi-channel attention-fusion neural network for brain age estimation: Accuracy, generality, and interpretation with 16,705 healthy MRIs across lifespan. *Med. Image Anal.* **72**, 102091 (2021).
8. E. Luders, N. Cherbuin, C. Gaser, Estimating brain age using high-resolution pattern recognition: Younger brains in long-term meditation practitioners. *Neuroimage* **134**, 508–513 (2016).
9. S. Mishra, I. Beheshti, P. Khanna, A review of neuroimaging-driven brain age estimation for identification of brain disorders and health conditions. *IEEE Rev. Biomed. Eng.* **16**, 371–385 (2023).
10. L. Baecker, R. Garcia-Dias, S. Vieira, C. Scarpazza, A. Mechelli, Machine learning for brain age prediction: Introduction to methods and clinical applications. *EBioMedicine* **72**, 103600 (2021).
11. H. Peng, W. Gong, C. F. Beckmann, A. Vedaldi, S. M. Smith, Accurate brain age prediction with lightweight deep neural networks. *Med. Image Anal.* **68**, 101871 (2021).
12. N. K. Dinsdale, E. Bluemke, S. M. Smith, Z. Arya, D. Vidaurre, M. Jenkinson, A. I. L. Namburete, Learning patterns of the ageing brain in MRI using deep convolutional networks. *Neuroimage* **224**, 117401 (2021).
13. H. Jiang, N. Lu, K. Chen, L. Yao, K. Li, J. Zhang, X. Guo, Predicting brain age of healthy adults based on structural MRI parcellation using convolutional neural networks. *Front. Neurol.* **10**, 1346 (2019).
14. K. M. Poloni, R. J. Ferrari, Alzheimer's Disease Neuroimaging Initiative, A deep ensemble hippocampal CNN model for brain age estimation applied to Alzheimer's diagnosis. *Expert Syst. Appl.* **195**, 116622 (2022).
15. J. Lee, B. J. Burkett, H.-K. Min, M. L. Senjem, E. S. Lundt, H. Botha, J. Graff-Radford, L. R. Barnard, J. L. Gunter, C. G. Schwarz, K. Kantarci, D. S. Knopman, B. F. Boeve, V. J. Lowe, R. C. Petersen, C. R. Jack Jr., D. T. Jones, Deep learning-based brain age prediction in normal aging and dementia. *Nat. Aging* **2**, 412–424 (2022).
16. S. He, P. E. Grant, Y. Ou, Global-local transformer for brain age estimation. *IEEE Trans. Med. Imaging* **41**, 213–224 (2022).
17. B. A. Jonsson, G. Bjornsdottir, T. E. Thorgeirsson, L. M. Ellingsen, G. B. Walters, D. F. Gudbjartsson, H. Stefansson, K. Stefansson, M. O. Ulfarsson, Brain age prediction using deep learning uncovers associated sequence variants. *Nat. Commun.* **10**, 5409 (2019).
18. A. Kolbeinsson, S. Filippi, Y. Panagakis, P. M. Matthews, P. Elliott, A. Dehghan, I. Tzoulaki, Accelerated MRI-predicted brain ageing and its associations with cardiometabolic and brain disorders. *Sci. Rep.* **10**, 19940 (2020).
19. W. Shi, G. Yan, Y. Li, H. Li, T. Liu, C. Sun, G. Wang, Y. Zhang, Y. Zou, D. Wu, Fetal brain age estimation and anomaly detection using attention-based deep ensembles with uncertainty. *Neuroimage* **223**, 117316 (2020).
20. K. Ning, L. Zhao, W. Matloff, F. Sun, A. W. Toga, Association of relative brain age with tobacco smoking, alcohol consumption, and genetic variants. *Sci. Rep.* **10**, 10 (2020).
21. S. M. Smith, L. T. Elliott, F. Alfaro-Almagro, P. McCarthy, T. E. Nichols, G. Douaud, K. L. Miller, Brain aging comprises many modes of structural and functional change with distinct genetic and biophysical associations. *Elife* **9**, e52677 (2020).
22. J. Wen, B. Zhao, Z. Yang, G. Erus, I. Skampardoni, E. Mamourian, Y. Cui, G. Hwang, J. Bao, A. Boquet-Pujadas, Z. Zhou, Y. Veturi, M. D. Ritchie, H. Shou, P. M. Thompson, L. Shen, A. W. Toga, C. Davatzikos, The genetic architecture of multimodal human brain age. *Nat. Commun.* **15**, 2604 (2024).
23. J. Wen, Y. E. Tian, I. Skampardoni, Z. Yang, E. Mamourian, F. Anagnostakis, B. Zhao, A. W. Toga, A. Zaleskey, C. Davatzikos, The genetic architecture of biological age in nine human organ systems. medRxiv 2023.06.08.23291168 [Preprint] (2023). https://doi.org/10.1101/2023.06.08.23291168.
24. E. H. Leonardsen, H. Peng, T. Kaufmann, I. Agartz, O. A. Andreassen, E. G. Celius, T. Espeseth, H. F. Harbo, E. A. Høgestøl, A.-M. de Lange, A. F. Marquand, D. Vidal-Piñeiro, J. M. Roe, G. Selbæk, Ø. Sørensen, S. M. Smith, L. T. Westlye, T. Wolfers, Y. Wang, Deep neural networks learn general and clinically relevant representations of the ageing brain. *Neuroimage* **256**, 119210 (2022).
25. T. Kaufmann, D. van der Meer, N. T. Doan, E. Schwarz, M. J. Lund, I. Agartz, D. Alnæs, D. M. Barch, R. Baur-Streubel, A. Bertolino, F. Bettella, M. K. Beyer, E. Bøen, S. Borgwardt, C. L. Brandt, J. Buitelaar, E. G. Celius, S. Cervenka, A. Conzelmann, A. Córdova-Palomera, A. M. Dale, D. J. F. de Quervain, P. Di Carlo, S. Djurovic, E. S. Dørum, S. Eisenacher, T. Elvsåshagen, T. Espeseth, H. Fatouros-Bergman, L. Flyckt, B. Franke, O. Frei, B. Haatveit, A. K. Håberg, H. F. Harbo, C. A. Hartman, D. Heslenfeld, P. J. Hoekstra, E. A. Høgestøl, T. L. Jernigan, R. Jonassen, E. G. Jönsson, Karolinska Schizophrenia Project (KaSP), P. Kirsch, I. Kłoszewska, K. K. Kolskår, N. I. Landrø, S. Le Hellard, K.-P. Lesch, S. Lovestone, A. Lundervold, A. J. Lundervold, L. A. Maglanoc, U. F. Malt, P. Mecocci, I. Melle, A. Meyer-Lindenberg, T. Moberget, L. B. Norbom, J. E. Nordvik, L. Nyberg, J. Oosterlaan, M. Papalino, A. Papassotiropoulos, P. Pauli, G. Pergola, K. Persson, G. Richard, J. Rokicki, A.-M. Sanders, G. Selbæk, A. A. Shadrin, O. B. Smeland, H. Soininen, P. Sowa, V. M. Steen, M. Tsolaki, K. M. Ulrichsen, B. Vellas, L. Wang, E. Westman, G. C. Ziegler, M. Zink, O. A. Andreassen, L. T. Westlye, Common brain disorders are associated with heritable patterns of apparent aging of the brain. *Nat. Neurosci.* **22**, 1617–1623 (2019).
26. J. H. Cole, S. J. Ritchie, M. E. Bastin, M. C. Valdés Hernández, S. Muñoz Maniega, N. Royle, J. Corley, A. Pattie, S. E. Harris, Q. Zhang, N. R. Wray, P. Redmond, R. E. Marioni, J. M. Starr, S. R. Cox, J. M. Wardlaw, D. J. Sharp, I. J. Deary, Brain age predicts mortality. *Mol. Psychiatry* **23**, 1385–1392 (2018).
27. J.-H. Jeong, J.-S. Jin, H.-N. Kim, S.-M. Kang, J. C. Liu, C. J. Lengner, F. Otto, S. Mundlos, J. L. Stein, A. J. van Wijnen, J. B. Lian, G. S. Stein, J.-Y. Choi, Expression of Runx2 transcription factor in non-skeletal tissues, sperm and brain. *J. Cell. Physiol.* **217**, 511–517 (2008).

28. B. K. Bulik-Sullivan, P.-R. Loh, H. K. Finucane, S. Ripke, J. Yang, Schizophrenia Working Group of the Psychiatric Genomics Consortium, N. Patterson, M. J. Daly, A. L. Price, B. M. Neale, LD Score regression distinguishes confounding from polygenicity in genome-wide association studies. *Nat. Genet.* **47**, 291–295 (2015).
29. Y. E. Tian, V. Cropley, A. B. Maier, N. T. Lautenschlager, M. Breakspear, A. Zalesky, Heterogeneous aging across multiple organ systems and prediction of chronic disease and mortality. *Nat. Med.* **29**, 1221–1231 (2023).
30. D. B. Rosoff, L. A. Mavromatis, A. S. Bell, J. Wagner, J. Jung, R. E. Marioni, G. Davey Smith, S. Horvath, F. W. Lohoff, Multivariate genome-wide analysis of aging-related traits identifies novel loci and new drug targets for healthy aging. *Nat. Aging* **3**, 1020–1035 (2023).
31. D. Mendez, A. Gaulton, A. P. Bento, J. Chambers, M. De Veij, E. Félix, M. P. Magariños, J. F. Mosquera, P. Mutowo, M. Nowotka, M. Gordillo-Marañón, F. Hunter, L. Junco, G. Mugumbate, M. Rodriguez-Lopez, F. Atkinson, N. Bosc, C. J. Radoux, A. Segura-Cabrera, A. Hersey, A. R. Leach, ChEMBL: Towards direct deposition of bioassay data. *Nucleic Acids Res.* **47**, D930–D940 (2019).
32. L. Partridge, M. Fuentealba, B. K. Kennedy, The quest to slow ageing through drug discovery. *Nat. Rev. Drug Discov.* **19**, 513–532 (2020).
33. A. S. Kulkarni, S. Aleksic, D. M. Berger, F. Sierra, G. A. Kuchel, N. Barzilai, Geroscience-guided repurposing of FDA-approved drugs to target aging: A proposed process and prioritization. *Aging Cell* **21**, e13596 (2022).
34. C. Finan, A. Gaulton, F. A. Kruger, R. T. Lumbers, T. Shah, J. Engmann, L. Galver, R. Kelley, A. Karlsson, R. Santos, J. P. Overington, A. D. Hingorani, J. P. Casas, The druggable genome and support for target identification and validation in drug development. *Sci. Transl. Med.* **9**, eaag1166 (2017).
35. C. Bycroft, C. Freeman, D. Petkova, G. Band, L. T. Elliott, K. Sharp, A. Motyer, D. Vukcevic, O. Delaneau, J. O'Connell, A. Cortes, S. Welsh, A. Young, M. Effingham, G. McVean, S. Leslie, N. Allen, P. Donnelly, J. Marchini, The UK Biobank resource with deep phenotyping and genomic data. *Nature* **562**, 203–209 (2018).
36. J. Lahoud, J. Cao, F. S. Khan, H. Cholakkal, R. M. Anwer, S. Khan, M.-H. Yang, 3D vision with transformers: A survey. arXiv:2208.04309 [cs.CV] (2022).
37. M. Gordillo-Marañón, M. Zwierzyna, P. Charoen, F. Drenos, S. Chopade, T. Shah, J. Engmann, N. Chaturvedi, O. Papacosta, G. Wannamethee, A. Wong, R. Sofat, M. Kivimaki, J. F. Price, A. D. Hughes, T. R. Gaunt, D. A. Lawlor, A. Gaulton, A. D. Hingorani, A. F. Schmidt, C. Finan, Validation of lipid-related therapeutic targets for coronary heart disease prevention using human genetics. *Nat. Commun.* **12**, 6120 (2021).
38. C. S. Storm, D. A. Kia, M. M. Almramhi, S. Bandres-Ciga, C. Finan, International Parkinson's Disease Genomics Consortium (IPDGC), A. D. Hingorani, N. W. Wood, Finding genetically-supported drug targets for Parkinson's disease using Mendelian randomization of the druggable genome. *Nat. Commun.* **12**, 7342 (2021).
39. A. F. Schmidt, C. Finan, M. Gordillo-Marañón, F. W. Asselbergs, D. F. Freitag, R. S. Patel, B. Tyl, S. Chopade, R. Faraway, M. Zwierzyna, A. D. Hingorani, Genetic drug target validation using Mendelian randomisation. *Nat. Commun.* **11**, 3255 (2020).
40. W. McLaren, L. Gil, S. E. Hunt, H. S. Riat, G. R. S. Ritchie, A. Thormann, P. Flicek, F. Cunningham, The Ensembl Variant Effect Predictor. *Genome Biol.* **17**, 122 (2016).
41. S. Cursano, C. R. Battaglia, C. Urrutia-Ruiz, S. Grabrucker, M. Schön, J. Bockmann, S. Braumüller, P. Radermacher, F. Roselli, M. Huber-Lang, T. M. Boeckers, A CRHR1 antagonist prevents synaptic loss and memory deficits in a trauma-induced delirium-like syndrome. *Mol. Psychiatry* **26**, 3778–3794 (2021).
42. M. Okamoto, K. Inoue, H. Iwamura, K. Terashima, H. Soya, M. Asashima, T. Kuwabara, Reduction in paracrine Wnt3 factors during aging causes impaired adult neurogenesis. *FASEB J.* **25**, 3570–3582 (2011).
43. L. He, Y. Loika, Y. Park, Genotype Tissue Expression (GTEx) consortium, D. A. Bennett, M. Kellis, A. M. Kulminski, Alzheimer's Disease Neuroimaging Initiative, Exome-wide age-of-onset analysis reveals exonic variants in *ERN1* and *SPPL2C* associated with Alzheimer's disease. *Transl. Psychiatry* **11**, 146 (2021).
44. T. Zhao, S. Ye, Z. Tang, L. Guo, Z. Ma, Y. Zhang, C. Yang, J. Peng, J. Chen, Loss-of-function of p53 isoform Δ113p53 accelerates brain aging in zebrafish. *Cell Death Dis.* **12**, 151 (2021).
45. D. Wu, C. Prives, Relevance of the p53-MDM2 axis to aging. *Cell Death Differ.* **25**, 169–179 (2018).
46. Y. D. Pettway, J. Walker, C. Dai, R. Aramandla, A. L. Hopkirk, C. Reihsmann, C. Davis, R. Jenkins, L. Sussel, S. Parker, A. C. Powers, M. Brissova, 231-OR: Reduced NKX2-2 expression enhances insulin secretion by primary human β-cells. *Diabetes* **72**, 10.2337/db23-231-OR (2023).
47. V. Zuber, N. F. Grinberg, D. Gill, I. Manipur, E. A. W. Slob, A. Patel, C. Wallace, S. Burgess, Combining evidence from Mendelian randomization and colocalization: Review and comparison of approaches. *Am. J. Hum. Genet.* **109**, 767–782 (2022).
48. W. A. Banks, M. J. Reed, A. F. Logsdon, E. M. Rhea, M. A. Erickson, Healthy aging and the blood-brain barrier. *Nat. Aging* **1**, 243–254 (2021).
49. G. L. Wallace, N. Dankner, L. Kenworthy, J. N. Giedd, A. Martin, Age-related temporal and parietal cortical thinning in autism spectrum disorders. *Brain* **133**, 3745–3754 (2010).
50. Q. Wang, X. Xu, M. Zhang, Normal aging in the basal ganglia evaluated by eigenvalues of diffusion tensor imaging. *AJNR Am. J. Neuroradiol.* **31**, 516–520 (2010).
51. C. J. Mummery, A. Börjesson-Hanson, D. J. Blackburn, E. G. B. Vijverberg, P. P. De Deyn, S. Ducharme, M. Jonsson, A. Schneider, J. O. Rinne, A. C. Ludolph, R. Bodenschatz, H. Kordasiewicz, E. E. Swayze, B. Fitzsimmons, L. Mignon, K. M. Moore, C. Yun, T. Baumann, D. Li, D. A. Norris, R. Crean, D. L. Graham, E. Huang, E. Ratti, C. F. Bennett, C. Junge, R. M. Lane, Tau-targeting antisense oligonucleotide $MAPT_{Rx}$ in mild Alzheimer's disease: A phase 1b, randomized, placebo-controlled trial. *Nat. Med.* **29**, 1437–1447 (2023).
52. A. Montagne, S. R. Barnes, M. D. Sweeney, M. R. Halliday, A. P. Sagare, Z. Zhao, A. W. Toga, R. E. Jacobs, C. Y. Liu, L. Amezcua, M. G. Harrington, H. C. Chui, M. Law, B. V. Zlokovic, Blood-brain barrier breakdown in the aging human hippocampus. *Neuron* **85**, 296–302 (2015).
53. Z. Yang, J. Wen, G. Erus, S. T. Govindarajan, R. Melhem, E. Mamourian, Y. Cui, D. Srinivasan, A. Abdulkadir, P. Parmpi, K. Wittfeld, H. J. Grabe, R. Bülow, S. Frenzel, D. Tosun, M. Bilgel, Y. An, D. Yi, D. S. Marcus, P. LaMontagne, T. L. S. Benzinger, S. R. Heckbert, T. R. Austin, S. R. Waldstein, M. K. Evans, A. B. Zonderman, L. J. Launer, A. Sotiras, M. A. Espeland, C. L. Masters, P. Maruff, J. Fripp, A. W. Toga, S. O'Bryant, M. M. Chakravarty, S. Villeneuve, S. C. Johnson, J. C. Morris, M. S. Albert, K. Yaffe, H. Völzke, L. Ferrucci, R. Nick Bryan, R. T. Shinohara, Y. Fan, M. Habes, P. A. Lalousis, N. Koutsouleris, D. A. Wolk, S. M. Resnick, H. Shou, I. M. Nasrallah, C. Davatzikos, Brain aging patterns in a large and diverse cohort of 49,482 individuals. *Nat. Med.* **30**, 3015–3026 (2024).
54. R. Migliaccio, F. Cacciamani, The temporal lobe in typical and atypical Alzheimer disease. *Handb. Clin. Neurol.* **187**, 449–466 (2022).
55. M. E. Murray, N. R. Graff-Radford, O. A. Ross, R. C. Petersen, R. Duara, D. W. Dickson, Neuropathologically defined subtypes of Alzheimer's disease with distinct clinical characteristics: A retrospective study. *Lancet Neurol.* **10**, 785–796 (2011).
56. K. A. Severson, L. M. Chahine, L. A. Smolensky, M. Dhuliawala, M. Frasier, K. Ng, S. Ghosh, J. Hu, Discovery of Parkinson's disease states and disease progression modelling: A longitudinal data study using machine learning. *Lancet Digit. Health* **3**, e555–e564 (2021).
57. D. Chen, X. Wang, V. Voon, Y. Jiang, C.-Y. Z. Lo, L. Wang, C. Shen, S. Xiang, S. Yao, J. Zhang, T. Jia, W. Cheng, J. Feng, Neurophysiological stratification of major depressive disorder by distinct trajectories. *Nat. Ment. Health* **1**, 863–875 (2023).
58. D. Stephan, O. Sbai, J. Wen, P.-O. Couraud, C. Putterman, M. Khrestchatisky, S. Desplat-Jégo, TWEAK/Fn14 pathway modulates properties of a human microvascular endothelial cell model of blood brain barrier. *J. Neuroinflammation* **10**, 9 (2013).
59. A. Vázquez-Carballo, V. Ceperuelo-Mallafré, M. R. Chacón, E. Maymó-Masip, M. Lorenzo, A. Porras, J. Vendrell, S. Fernández-Veledo, TWEAK prevents TNF-α-induced insulin resistance through PP2A activation in human adipocytes. *Am. J. Physiol. Endocrinol. Metab.* **305**, E101–E112 (2013).
60. T. F. Galatro, I. R. Holtman, A. M. Lerario, I. D. Vainchtein, N. Brouwer, P. R. Sola, M. M. Veras, T. F. Pereira, R. E. P. Leite, T. Möller, P. D. Wes, M. C. Sogayar, J. D. Laman, W. den Dunnen, C. A. Pasqualucci, S. M. Oba-Shinjo, E. W. G. M. Boddeke, S. K. N. Marie, B. J. L. Eggen, Transcriptomic analysis of purified human cortical microglia reveals age-associated changes. *Nat. Neurosci.* **20**, 1162–1171 (2017).
61. S. Hiroyasu, M. R. Zeglinski, H. Zhao, M. A. Pawluk, C. T. Turner, A. Kasprick, C. Tateishi, W. Nishie, A. Burleigh, P. A. Lennox, N. Van Laeken, N. J. Carr, F. Petersen, R. I. Crawford, H. Shimizu, D. Tsuruta, R. J. Ludwig, D. J. Granville, Granzyme B inhibition reduces disease severity in autoimmune blistering diseases. *Nat. Commun.* **12**, 302 (2021).
62. C. T. Turner, J. Bolsoni, M. R. Zeglinski, H. Zhao, T. Ponomarev, K. Richardson, S. Hiroyasu, E. Schmid, A. Papp, D. J. Granville, Granzyme B mediates impaired healing of pressure injuries in aged skin. *NPJ Aging Mech. Dis.* **7**, 6 (2021).
63. C. T. Turner, D. Lim, D. J. Granville, Granzyme B in skin inflammation and disease. *Matrix Biol.* **75–76**, 126–140 (2019).
64. X. Li, C. Li, W. Zhang, Y. Wang, P. Qian, H. Huang, Inflammation and aging: Signaling pathways and intervention therapies. *Signal Transduct. Target. Ther.* **8**, 239 (2023).
65. S. Shen, C. Li, L. Xiao, X. Wang, H. Lv, Y. Shi, Y. Li, Q. Huang, Whole-genome sequencing of Chinese centenarians reveals important genetic variants in aging WGS of centenarian for genetic analysis of aging. *Hum. Genomics* **14**, 23 (2020).
66. L. Bouchard, V. Drapeau, V. Provencher, S. Lemieux, Y. Chagnon, T. Rice, D. C. Rao, M.-C. Vohl, A. Tremblay, C. Bouchard, L. Pérusse, Neuromedin β: A strong candidate gene linking eating behaviors and susceptibility to obesity. *Am. J. Clin. Nutr.* **80**, 1478–1486 (2004).
67. A. Drewnowski, J. M. Shultz, Impact of aging on eating behaviors, food choices, nutrition, and health status. *J. Nutr. Health Aging* **5**, 75–79 (2001).
68. Y. Coudert, V. A. T. Le, H. Adam, M. Bès, F. Vignols, S. Jouannic, E. Guiderdoni, P. Gantet, Identification of CROWN ROOTLESS1-regulated genes in rice reveals specific and conserved elements of postembryonic root formation. *New Phytol.* **206**, 243–254 (2015).
69. P. Wang, L. Jin, M. Zhang, Y. Wu, Z. Duan, Y. Guo, C. Wang, Y. Guo, W. Chen, Z. Liao, Y. Wang, R. Lai, L. P. Lee, J. Qin, Blood-brain barrier injury and neuroinflammation induced by SARS-CoV-2 in a lung-brain microphysiological system. *Nat. Biomed. Eng.* **8**, 1053–1068 (2023).

70. M. F. Gulen, N. Samson, A. Keller, M. Schwabenland, C. Liu, S. Glück, V. V. Thacker, L. Favre, B. Mangeat, L. J. Kroese, P. Krimpenfort, M. Prinz, A. Ablasser, cGAS-STING drives ageing-related inflammation and neurodegeneration. *Nature* **620**, 374–380 (2023).
71. N. Szuber, C. A. Hanson, T. L. Lasho, C. Finke, R. P. Ketterling, A. Pardanani, N. Gangat, A. Tefferi, MPL-mutated essential thrombocythemia: A morphologic reappraisal. *Blood Cancer J.* **8**, 121 (2018).
72. C. Li, Y. Zhu, Y. Ma, R. Hua, B. Zhong, W. Xie, Association of cumulative blood pressure with cognitive decline, dementia, and mortality. *J. Am. Coll. Cardiol.* **79**, 1321–1335 (2022).
73. R. Fernández-Jiménez, C. Real, Optimizing blood pressure components for a healthy brain: The holy grail in blood pressure management. *J. Am. Coll. Cardiol.* **79**, 1336–1339 (2022).
74. A. C. Yang, M. Y. Stevens, M. B. Chen, D. P. Lee, D. Stähli, D. Gate, K. Contrepois, W. Chen, T. Iram, L. Zhang, R. T. Vest, A. Chaney, B. Lehallier, N. Olsson, H. du Bois, R. Hsieh, H. C. Cropper, D. Berdnik, L. Li, E. Y. Wang, G. M. Traber, C. R. Bertozzi, J. Luo, M. P. Snyder, J. E. Elias, S. R. Quake, M. L. James, T. Wyss-Coray, Physiological blood-brain transport is impaired with age by a shift in transcytosis. *Nature* **583**, 425–430 (2020).
75. E. R. L. C. Vardy, K. A. B. Kellett, S. L. Cocklin, N. M. Hooper, Alkaline phosphatase is increased in both brain and plasma in Alzheimer's disease. *Neurodegener. Dis.* **9**, 31–37 (2012).
76. R. Romaniello, F. Arrigoni, A. E. Fry, M. T. Bassi, M. I. Rees, R. Borgatti, D. T. Pilz, T. D. Cushion, Tubulin genes and malformations of cortical development. *Eur. J. Med. Genet.* **61**, 744–754 (2018).
77. Y. Chang, Y. Zhou, J. Zhou, W. Li, J. Cao, Y. Jing, S. Zhang, Y. Shen, Q. Lin, X. Fan, H. Yang, X. Dong, S. Zhang, X. Yi, L. Shuai, L. Shi, Z. Liu, J. Yang, X. Ma, J. Hao, K. Chen, M. J. Li, F. Wang, D. Huang, Unraveling the causal genes and transcriptomic determinants of human telomere length. *Nat. Commun.* **14**, 8517 (2023).
78. T. F. Shay, E. E. Sullivan, X. Ding, X. Chen, S. Ravindra Kumar, D. Goertsen, D. Brown, A. Crosby, J. Vielmetter, M. Borsos, D. A. Wolfe, A. W. Lam, V. Gradinaru, Primate-conserved carbonic anhydrase IV and murine-restricted LY6C1 enable blood-brain barrier crossing by engineered viral vectors. *Sci. Adv.* **9**, eadg6618 (2023).
79. D. Wang, E. A. Day, L. K. Townsend, D. Djordjevic, S. B. Jørgensen, G. R. Steinberg, GDF15: Emerging biology and therapeutic applications for obesity and cardiometabolic disease. *Nat. Rev. Endocrinol.* **17**, 592–607 (2021).
80. A. Didonna, Tau at the interface between neurodegeneration and neuroinflammation. *Genes Immun.* **21**, 288–300 (2020).
81. M. Simon, M. Van Meter, J. Ablaeva, Z. Ke, R. S. Gonzalez, T. Taguchi, M. De Cecco, K. I. Leonova, V. Kogan, S. L. Helfand, N. Neretti, A. Roichman, H. Y. Cohen, M. V. Meer, V. N. Gladyshev, M. P. Antoch, A. V. Gudkov, J. M. Sedivy, A. Seluanov, V. Gorbunova, LINE1 derepression in aged wild-type and SIRT6-deficient mice drives inflammation. *Cell Metab.* **29**, 871–885.e5 (2019).
82. P. Juricic, Y.-X. Lu, T. Leech, L. F. Drews, J. Paulitz, J. Lu, T. Nespital, S. Azami, J. C. Regan, E. Funk, J. Fröhlich, S. Grönke, L. Partridge, Long-lasting geroprotection from brief rapamycin treatment in early adulthood by persistently increased intestinal autophagy. *Nat. Aging* **2**, 824–836 (2022).
83. J. B. Mannick, D. W. Lamming, Targeting the biology of aging with mTOR inhibitors. *Nat. Aging* **3**, 642–660 (2023).
84. M. Bonaccio, A. Di Castelnuovo, S. Costanzo, A. De Curtis, M. B. Donati, C. Cerletti, G. de Gaetano, L. Iacoviello, MOLI-SANI Investigators, Age-sex-specific ranges of platelet count and all-cause mortality: Prospective findings from the MOLI-SANI study. *Blood* **127**, 1614–1616 (2016).
85. V. Todorovic, Platelets rejuvenate the aging brain. *Nat. Cardiovasc. Res.* **2**, 859 (2023).
86. A. B. Schroer, P. B. Ventura, J. Sucharov, R. Misra, M. K. K. Chui, G. Bieri, A. M. Horowitz, L. K. Smith, K. Encabo, I. Tenggara, J. Couthouis, J. D. Gross, J. M. Chan, A. Luke, S. A. Villeda, Platelet factors attenuate inflammation and rescue cognition in ageing. *Nature* **620**, 1071–1079 (2023).
87. C. Park, O. Hahn, S. Gupta, A. J. Moreno, F. Marino, B. Kedir, D. Wang, S. A. Villeda, T. Wyss-Coray, D. B. Dubal, Platelet factors are induced by longevity factor klotho and enhance cognition in young and aging mice. *Nat. Aging* **3**, 1067–1078 (2023).
88. O. Leiter, D. Brici, S. J. Fletcher, X. L. H. Yong, J. Widagdo, N. Matigian, A. B. Schroer, G. Bieri, D. G. Blackmore, P. F. Bartlett, V. Anggono, S. A. Villeda, T. L. Walker, Platelet-derived exerkine CXCL4/platelet factor 4 rejuvenates hippocampal neurogenesis and restores cognitive function in aged mice. *Nat. Commun.* **14**, 4375 (2023).
89. T. Wyss-Coray, Ageing, neurodegeneration and brain rejuvenation. *Nature* **539**, 180–186 (2016).
90. G. Bieri, A. B. Schroer, S. A. Villeda, Blood-to-brain communication in aging and rejuvenation. *Nat. Neurosci.* **26**, 379–393 (2023).
91. B. Taschler, S. M. Smith, T. E. Nichols, Causal inference on neuroimaging data with Mendelian randomisation. *Neuroimage* **258**, 119385 (2022).
92. M.-G. Duperron, M. J. Knol, Q. Le Grand, T. E. Evans, A. Mishra, A. Tsuchida, G. Roshchupkin, T. Konuma, D.-A. Trégouët, J. R. Romero, S. Frenzel, M. Luciano, E. Hofer, M. Bourgey, N. D. Dueker, P. Delgado, S. Hilal, R. M. Tankard, F. Dubost, J. Shin, Y. Saba, N. J. Armstrong, C. Bordes, M. E. Bastin, A. Beiser, H. Brodaty, R. Bülow, C. Carrera, C. Chen, C.-Y. Cheng, I. J. Deary, P. G. Gampawar, J. J. Himali, J. Jiang, T. Kawaguchi, S. Li, M. Macalli, P. Marquis, Z. Morris, S. M. Maniega, S. Miyamoto, M. Okawa, M. Paradise, P. Parva, T. Rundek, M. Sargurupremraj, S. Schilling, K. Setoh, O. Soukarieh, Y. Tabara, A. Teumer, A. Thalamuthu, J. N. Trollor, M. C. V. Hernández, M. W. Vernooij, U. Völker, K. Wittfeld, T. Y. Wong, M. J. Wright, J. Zhang, W. Zhao, Y.-C. Zhu, H. Schmidt, P. S. Sachdev, W. Wen, K. Yoshida, A. Joutel, C. L. Satizabal, R. L. Sacco, G. Bourque, CHARGE consortium, M. Lathrop, T. Paus, I. Fernandez-Cadenas, Q. Yang, B. Mazoyer, P. Boutinaud, Y. Okada, H. J. Grabe, K. A. Mather, R. Schmidt, M. Joliot, M. A. Ikram, F. Matsuda, C. Tzourio, J. M. Wardlaw, S. Seshadri, H. H. H. Adams, S. Debette, Genomics of perivascular space burden unravels early mechanisms of cerebral small vessel disease. *Nat. Med.* **29**, 950–962 (2023).
93. J. Sepulcre, M. J. Grothe, F. d'Oleire Uquillas, L. Ortiz-Terán, I. Diez, H.-S. Yang, H. I. L. Jacobs, B. J. Hanseeuw, Q. Li, G. El-Fakhri, R. A. Sperling, K. A. Johnson, Neurogenetic contributions to amyloid beta and tau spreading in the human cortex. *Nat. Med.* **24**, 1910–1918 (2018).
94. M. W. Woolrich, S. Jbabdi, B. Patenaude, M. Chappell, S. Makni, T. Behrens, C. Beckmann, M. Jenkinson, S. M. Smith, Bayesian analysis of neuroimaging data in FSL. *Neuroimage* **45**, S173–S186 (2009).
95. S. M. Smith, M. Jenkinson, M. W. Woolrich, C. F. Beckmann, T. E. J. Behrens, H. Johansen-Berg, P. R. Bannister, M. De Luca, I. Drobnjak, D. E. Flitney, R. K. Niazy, J. Saunders, J. Vickers, Y. Zhang, N. De Stefano, J. M. Brady, P. M. Matthews, Advances in functional and structural MR image analysis and implementation as FSL. *Neuroimage* **23**, S208–S219 (2004).
96. A. Dosovitskiy, L. Beyer, A. Kolesnikov, D. Weissenborn, X. Zhai, T. Unterthiner, M. Dehghani, M. Minderer, G. Heigold, S. Gelly, J. Uszkoreit, N. Houlsby, An image is worth 16x16 words: Transformers for image recognition at scale. arXiv:2010.11929 [cs.CV] (2020).
97. L. T. Elliott, K. Sharp, F. Alfaro-Almagro, S. Shi, K. L. Miller, G. Douaud, J. Marchini, S. M. Smith, Genome-wide association studies of brain imaging phenotypes in UK Biobank. *Nature* **562**, 210–216 (2018).
98. K. Watanabe, E. Taskesen, A. van Bochoven, D. Posthuma, Functional mapping and annotation of genetic associations with FUMA. *Nat. Commun.* **8**, 1826 (2017).
99. R. Malik, G. Chauhan, M. Traylor, M. Sargurupremraj, Y. Okada, A. Mishra, L. Rutten-Jacobs, A.-K. Giese, S. W. van der Laan, S. Gretarsdottir, C. D. Anderson, M. Chong, H. H. H. Adams, T. Ago, P. Almgren, P. Amouyel, H. Ay, T. M. Bartz, O. R. Benavente, S. Bevan, G. B. Boncoraglio, R. D. Brown Jr., A. S. Butterworth, C. Carrera, C. L. Carty, D. I. Chasman, W.-M. Chen, J. W. Cole, A. Correa, I. Cotlarciuc, C. Cruchaga, J. Danesh, P. I. W. de Bakker, A. L. De Stefano, M. den Hoed, Q. Duan, S. T. Engelter, G. J. Falcone, R. F. Gottesman, R. P. Grewal, V. Gudnason, S. Gustafsson, J. Haessler, T. B. Harris, A. Hassan, A. S. Havulinna, S. R. Heckbert, E. G. Holliday, G. Howard, F.-C. Hsu, H. I. Hyacinth, M. A. Ikram, E. Ingelsson, M. R. Irvin, X. Jian, J. Jiménez-Conde, J. A. Johnson, J. W. Jukema, M. Kanai, K. L. Keene, B. M. Kissela, D. O. Kleindorfer, C. Kooperberg, M. Kubo, L. A. Lange, C. D. Langefeld, C. Langenberg, L. J. Launer, J.-M. Lee, R. Lemmens, D. Leys, C. M. Lewis, W.-Y. Lin, A. G. Lindgren, E. Lorentzen, P. K. Magnusson, J. Maguire, A. Manichaikul, P. F. M. Ardle, J. F. Meschia, B. D. Mitchell, T. H. Mosley, M. A. Nalls, T. Ninomiya, M. J. O'Donnell, B. M. Psaty, S. L. Pulit, K. Rannikmäe, A. P. Reiner, K. M. Rexrode, K. Rice, S. S. Rich, P. M. Ridker, N. S. Rost, P. M. Rothwell, J. I. Rotter, T. Rundek, R. L. Sacco, S. Sakaue, M. M. Sale, V. Salomaa, B. R. Sapkota, R. Schmidt, C. O. Schmidt, U. Schminke, P. Sharma, A. Slowik, C. L. M. Sudlow, C. Tanislav, T. Tatlisumak, K. D. Taylor, V. N. S. Thijs, G. Thorleifsson, U. Thorsteinsdottir, S. Tiedt, S. Trompet, C. Tzourio, C. M. van Duijn, M. Walters, N. J. Wareham, S. Wassertheil-Smoller, J. G. Wilson, K. L. Wiggins, Q. Yang, S. Yusuf, AFGen Consortium, Cohorts for Heart and Aging Research in Genomic Epidemiology (CHARGE) Consortium, International Genomics of Blood Pressure (iGEN-BP) Consortium, INVENT Consortium, STARNET, J. C. Bis, T. Pastinen, A. Ruusalepp, E. E. Schadt, S. Koplev, J. L. M. Björkegren, V. Codoni, M. Civelek, N. L. Smith, D. A. Trégouët, I. E. Christophersen, C. Roselli, S. A. Lubitz, P. T. Ellinor, E. S. Tai, J. S. Kooner, N. Kato, J. He, P. van der Harst, P. Elliott, J. C. Chambers, F. Takeuchi, A. D. Johnson, BioBank Japan Cooperative Hospital Group, COMPASS Consortium, EPIC-CVD Consortium, EPIC-InterAct Consortium, International Stroke Genetics Consortium (ISGC), METASTROKE Consortium, Neurology Working Group of the CHARGE Consortium, NINDS Stroke Genetics Network (SiGN), UK Young Lacunar DNA Study, MEGASTROKE Consortium, D. K. Sanghera, O. Melander, C. Jern, D. Strbian, I. Fernandez-Cadenas, W. T. Longstreth Jr., A. Rolfs, J. Hata, D. Woo, J. Rosand, G. Pare, J. C. Hopewell, D. Saleheen, K. Stefansson, B. B. Worrall, S. J. Kittner, S. Seshadri, M. Fornage, H. S. Markus, J. M. M. Howson, Y. Kamatani, S. Debette, M. Dichgans, Multiancestry genome-wide association study of 520,000 subjects identifies 32 loci associated with stroke and stroke subtypes. *Nat. Genet.* **50**, 524–537 (2018).
100. C. A. Rietveld, S. E. Medland, J. Derringer, J. Yang, T. Esko, N. W. Martin, H.-J. Westra, K. Shakhbazov, A. Abdellaoui, A. Agrawal, E. Albrecht, B. Z. Alizadeh, N. Amin, J. Barnard, S. E. Baumeister, K. S. Benke, L. F. Bielak, J. A. Boatman, P. A. Boyle, G. Davies, C. de Leeuw, N. Eklund, D. S. Evans, R. Ferhmann, K. Fischer, C. Gieger, H. K. Gjessing, S. Hägg, J. R. Harris, C. Hayward, C. Holzapfel, C. A. Ibrahim-Verbaas, E. Ingelsson, B. Jacobsson, P. K. Joshi, A. Jugessur, M. Kaakinen, S. Kanoni, J. Karjalainen, I. Kolcic, K. Kristiansson, Z. Kutalik, J. Lahti, S. H. Lee, P. Lin, P. A. Lind, Y. Liu, K. Lohman, M. Loitfelder, G. McMahon,

P. M. Vidal, O. Meirelles, L. Milani, R. Myhre, M.-L. Nuotio, C. J. Oldmeadow, K. E. Petrovic, W. J. Peyrot, O. Polasek, L. Quaye, E. Reinmaa, J. P. Rice, T. S. Rizzi, H. Schmidt, R. Schmidt, A. V. Smith, J. A. Smith, T. Tanaka, A. Terracciano, M. J. H. M. van der Loos, V. Vitart, H. Völzke, J. Wellmann, L. Yu, W. Zhao, J. Allik, J. R. Attia, S. Bandinelli, F. Bastardot, J. Beauchamp, D. A. Bennett, K. Berger, L. J. Bierut, D. I. Boomsma, U. Bültmann, H. Campbell, C. F. Chabris, L. Cherkas, M. K. Chung, F. Cucca, M. de Andrade, P. L. De Jager, J.-E. De Neve, I. J. Deary, G. V. Dedoussis, P. Deloukas, M. Dimitriou, G. Eiríksdóttir, M. F. Elderson, J. G. Eriksson, D. M. Evans, J. D. Faul, L. Ferrucci, M. E. Garcia, H. Grönberg, V. Guðnason, P. Hall, J. M. Harris, T. B. Harris, N. D. Hastie, A. C. Heath, D. G. Hernandez, W. Hoffmann, A. Hofman, R. Holle, E. G. Holliday, J.-J. Hottenga, W. G. Iacono, T. Illig, M.-R. Järvelin, M. Kähönen, J. Kaprio, R. M. Kirkpatrick, M. Kowgier, A. Latvala, L. J. Launer, D. A. Lawlor, T. Lehtimäki, J. Li, P. Lichtenstein, P. Lichtner, D. C. Liewald, P. A. Madden, P. K. E. Magnusson, T. E. Mäkinen, M. Masala, M. McGue, A. Metspalu, A. Mielck, M. B. Miller, G. W. Montgomery, S. Mukherjee, D. R. Nyholt, B. A. Oostra, L. J. Palmer, A. Palotie, B. W. J. H. Penninx, M. Perola, P. A. Peyser, M. Preisig, K. Räikkönen, O. T. Raitakari, A. Realo, S. M. Ring, S. Ripatti, F. Rivadeneira, I. Rudan, A. Rustichini, V. Salomaa, A.-P. Sarin, D. Schlessinger, R. J. Scott, H. Snieder, B. S. Pourcain, J. M. Starr, J. H. Sul, I. Surakka, R. Svento, A. Teumer, LifeLines Cohort Study, H. Tiemeier, F. J. A. van Rooij, D. R. Van Wagoner, E. Vartiainen, J. Viikari, P. Vollenweider, J. M. Vonk, G. Waeber, D. R. Weir, H.-E. Wichmann, E. Widen, G. Willemsen, J. F. Wilson, A. F. Wright, D. Conley, G. Davey-Smith, L. Franke, P. J. F. Groenen, A. Hofman, M. Johannesson, S. L. R. Kardia, R. F. Krueger, D. Laibson, N. G. Martin, M. N. Meyer, D. Posthuma, A. R. Thurik, N. J. Timpson, A. G. Uitterlinden, C. M. van Duijn, P. M. Visscher, D. J. Benjamin, D. Cesarini, P. D. Koellinger, GWAS of 126,559 individuals identifies genetic variants associated with educational attainment. *Science* **340**, 1467–1471 (2013).

101. U. Võsa, A. Claringbould, H.-J. Westra, M. J. Bonder, P. Deelen, B. Zeng, H. Kirsten, A. Saha, R. Kreuzhuber, S. Yazar, H. Brugge, R. Oelen, D. H. de Vries, M. G. P. van der Wijst, S. Kasela, N. Pervjakova, I. Alves, M.-J. Favé, M. Agbessi, M. W. Christiansen, R. Jansen, I. Seppälä, L. Tong, A. Teumer, K. Schramm, G. Hemani, J. Verlouw, H. Yaghootkar, R. S. Flitman, A. Brown, V. Kukushkina, A. Kalnapenkis, S. Rüeger, E. Porcu, J. Kronberg, J. Kettunen, B. Lee, F. Zhang, T. Qi, J. A. Hernandez, W. Arindrarto, F. Beutner, BIOS Consortium, i2QTL Consortium, J. Dmitrieva, M. Elansary, B. P. Fairfax, M. Georges, B. T. Heijmans, A. W. Hewitt, M. Kähönen, Y. Kim, J. C. Knight, P. Kovacs, K. Krohn, S. Li, M. Loeffler, U. M. Marigorta, H. Mei, Y. Momozawa, M. Müller-Nurasyid, M. Nauck, M. G. Nivard, B. W. J. H. Penninx, J. K. Pritchard, O. T. Raitakari, O. Rotzschke, E. P. Slagboom, C. D. A. Stehouwer, M. Stumvoll, P. Sullivan, P. A. C. 't Hoen, J. Thiery, A. Tönjes, J. van Dongen, M. van Iterson, J. H. Veldink, U. Völker, R. Warmerdam, C. Wijmenga, M. Swertz, A. Andiappan, G. W. Montgomery, S. Ripatti, M. Perola, Z. Kutalik, E. Dermitzakis, S. Bergmann, T. Frayling, J. van Meurs, H. Prokisch, H. Ahsan, B. L. Pierce, T. Lehtimäki, D. I. Boomsma, B. M. Psaty, S. A. Gharib, P. Awadalla, L. Milani, W. H. Ouwehand, K. Downes, O. Stegle, A. Battle, P. M. Visscher, J. Yang, M. Scholz, J. Powell, G. Gibson, T. Esko, L. Franke, Large-scale cis- and trans-eQTL analyses identify thousands of genetic loci and polygenic scores that regulate blood gene expression. *Nat. Genet.* **53**, 1300–1310 (2021).
102. D. Wang, S. Liu, J. Warrell, H. Won, X. Shi, F. C. P. Navarro, D. Clarke, M. Gu, P. Emani, Y. T. Yang, M. Xu, M. J. Gandal, S. Lou, J. Zhang, J. J. Park, C. Yan, S. K. Rhie, K. Manakongtreecheep, H. Zhou, A. Nathan, M. Peters, E. Mattei, D. Fitzgerald, T. Brunetti, J. Moore, Y. Jiang, K. Girdhar, G. E. Hoffman, S. Kalayci, Z. H. Gümüş, G. E. Crawford, PsychENCODE Consortium, P. Roussos, S. Akbarian, A. E. Jaffe, K. P. White, Z. Weng, N. Sestan, D. H. Geschwind, J. A. Knowles, M. B. Gerstein, Comprehensive functional genomic resource and integrative model for the human brain. *Science* **362**, eaat8464 (2018).
103. GTEx Consortium, Human genomics. The Genotype-Tissue Expression (GTEx) pilot analysis: Multitissue gene regulation in humans. *Science* **348**, 648–660 (2015).
104. Z. Yuan, H. Zhu, P. Zeng, S. Yang, S. Sun, C. Yang, J. Liu, X. Zhou, Testing and controlling for horizontal pleiotropy with probabilistic Mendelian randomization in transcriptome-wide association studies. *Nat. Commun.* **11**, 3861 (2020).
105. T. Wu, E. Hu, S. Xu, M. Chen, P. Guo, Z. Dai, T. Feng, L. Zhou, W. Tang, L. Zhan, X. Fu, S. Liu, X. Bo, G. Yu, clusterProfiler 4.0: A universal enrichment tool for interpreting omics data. *Innovation* **2**, 100141 (2021).
106. J. Zheng, V. Haberland, D. Baird, V. Walker, P. C. Haycock, M. R. Hurle, A. Gutteridge, P. Erola, Y. Liu, S. Luo, J. Robinson, T. G. Richardson, J. R. Staley, B. Elsworth, S. Burgess, B. B. Sun, J. Danesh, H. Runz, J. C. Maranville, H. M. Martin, J. Yarmolinsky, C. Laurin, M. V. Holmes, J. Z. Liu, K. Estrada, R. Santos, L. McCarthy, D. Waterworth, M. R. Nelson, G. D. Smith, A. S. Butterworth, G. Hemani, R. A. Scott, T. R. Gaunt, Phenome-wide Mendelian randomization mapping the influence of the plasma proteome on complex diseases. *Nat. Genet.* **52**, 1122–1131 (2020).
107. B. B. Sun, J. C. Maranville, J. E. Peters, D. Stacey, J. R. Staley, J. Blackshaw, S. Burgess, T. Jiang, E. Paige, P. Surendran, C. Oliver-Williams, M. A. Kamat, B. P. Prins, S. K. Wilcox, E. S. Zimmerman, A. Chi, N. Bansal, S. L. Spain, A. M. Wood, N. W. Morrell, J. R. Bradley, N. Janjic, D. J. Roberts, W. H. Ouwehand, J. A. Todd, N. Soranzo, K. Suhre, D. S. Paul, C. S. Fox, R. M. Plenge, J. Danesh, H. Runz, A. S. Butterworth, Genomic atlas of the human plasma proteome. *Nature* **558**, 73–79 (2018).
108. E. Ferkingstad, P. Sulem, B. A. Atlason, G. Sveinbjornsson, M. I. Magnusson, E. L. Styrmisdottir, K. Gunnarsdottir, A. Helgason, A. Oddsson, B. V. Halldorsson, B. O. Jensson, F. Zink, G. H. Halldorsson, G. Masson, G. A. Arnadottir, H. Katrinardottir, K. Juliusson, M. K. Magnusson, O. T. Magnusson, R. Fridriksdottir, S. Saevarsdottir, S. A. Gudjonsson, S. N. Stacey, S. Rognvaldsson, T. Eiriksdottir, T. A. Olafsdottir, V. Steinthorsdottir, V. Tragante, M. O. Ulfarsson, H. Stefansson, I. Jonsdottir, H. Holm, T. Rafnar, P. Melsted, J. Saemundsdottir, G. L. Norddahl, S. H. Lund, D. F. Gudbjartsson, U. Thorsteinsdottir, K. Stefansson, Large-scale integration of the plasma proteome with genetics and disease. *Nat. Genet.* **53**, 1712–1721 (2021).
109. K. C. Cotto, A. H. Wagner, Y.-Y. Feng, S. Kiwala, A. C. Coffman, G. Spies, A. Wollam, N. C. Spies, O. L. Griffith, M. Griffith, DGIdb 3.0: A redesign and expansion of the drug-gene interaction database. *Nucleic Acids Res.* **46**, D1068–D1073 (2018).
110. D. S. Wishart, Y. D. Feunang, A. C. Guo, E. J. Lo, A. Marcu, J. R. Grant, T. Sajed, D. Johnson, C. Li, Z. Sayeeda, N. Assempour, I. Iynkkaran, Y. Liu, A. Maciejewski, N. Gale, A. Wilson, L. Chin, R. Cummings, D. Le, A. Pon, C. Knox, M. Wilson, DrugBank 5.0: A major update to the DrugBank database for 2018. *Nucleic Acids Res.* **46**, D1074–D1082 (2018).
111. B. Lehallier, D. Gate, N. Schaum, T. Nanasi, S. E. Lee, H. Yousef, P. Moran Losada, D. Berdnik, A. Keller, J. Verghese, S. Sathyan, C. Franceschi, S. Milman, N. Barzilai, T. Wyss-Coray, Undulating changes in human plasma proteome profiles across the lifespan. *Nat. Med.* **25**, 1843–1850 (2019).
112. F. E. Wiklund, A. M. Bennet, P. K. E. Magnusson, U. K. Eriksson, F. Lindmark, L. Wu, N. Yaghoutyfam, C. P. Marquis, P. Stattin, N. L. Pedersen, H.-O. Adami, H. Grönberg, S. N. Breit, D. A. Brown, Macrophage inhibitory cytokine-1 (MIC-1/GDF15): A new marker of all-cause mortality. *Aging Cell* **9**, 1057–1064 (2010).
113. M. Conte, C. Giuliani, A. Chiariello, V. Iannuzzi, C. Franceschi, S. Salvioli, GDF15, an emerging key player in human aging. *Ageing Res. Rev.* **75**, 101569 (2022).
114. F. Laezza, T. J. Wilding, S. Sequeira, F. Coussen, X. Z. Zhang, R. Hill-Robinson, C. Mulle, J. E. Huettner, A. M. Craig, KRIP6: A novel BTB/kelch protein regulating function of kainate receptors. *Mol. Cell. Neurosci.* **34**, 539–550 (2007).
115. X. Han, Y.-J. Liu, B.-W. Liu, Z.-L. Ma, T.-J. Xia, X.-P. Gu, TREM2 and CD163 ameliorate microglia-mediated inflammatory environment in the aging brain. *J. Mol. Neurosci.* **72**, 1075–1084 (2022).
116. A. Mann, S. L. Miksys, A. Gaedigk, S. J. Kish, D. C. Mash, R. F. Tyndale, The neuroprotective enzyme CYP2D6 increases in the brain with age and is lower in Parkinson's disease patients. *Neurobiol. Aging* **33**, 2160–2171 (2012).

Acknowledgments: The UKB resource was used under application number 89757. The MEGASTROKE project received funding from sources specified at https://www.megastroke.org/acknowledgements.html. We would like to thank the editor and reviewers for constructive suggestions on the manuscript and J. Yang from Westlake University for assisting in the interpretation of GWAS statistical power and heritability. **Funding:** This work was partially supported by the National Key Research and Development Program of China under grant no. 2022YFF1202400, National Nature Science Foundation of China under grant no. 82272129, and Science Foundation for 3+1 Young Scholars of Chinese PLA General Hospital under grant no. 20230435. **Author contributions:** Conceptualization: Z.H. and Z.J. Methodology: Z.H., Z.J., and F.Y. Software: F.Y. and Z.J. Validation: F.Y., Z.J., and Y.-C.Z. Investigation: F.Y., Z.J., J.Y., M.P., J.S., F.W., Y.-C.Z., and Z.H. Data curation: F.Y. and Z.J. Visualization: F.Y. and Z.J. Supervision: Z.H., F.W., and Y.-C.Z. Writing—original draft: F.Y., Z.J., M.P., Y.-C.Z., and Z.H. Writing—review and editing: F.Y., Z.J., M.P., Y.-C.Z., Z.H., and F.W. **Competing interests:** The authors declare that they have no competing interests. **Data and materials availability:** The data that support training and validating the proposed brain age estimation model were obtained from the UKB (https://ukbiobank.ac.uk/enable-your-research/register), the Information eXtraction from Images (IXI) dataset (https://brain-development.org/ixi-dataset/), the Alzheimer's Disease Neuroimaging Initiative (ADNI) dataset (https://adni.loni.usc.edu/), and the Parkinson's Progression Markers Initiative (PPMI) dataset (https://ppmi-info.org/), upon registration and compliance with the data use agreement. Tissue-specific eQTL data were obtained from the eQTLGen (https://eqtlgen.org/) and PsychENCODE consortia (http://resource.psychencode.org/). pQTL data were obtained from the INTERVAL study (https://www.ebi.ac.uk/gwas/publications/29875488) and the deCODE study (https://decode.com/). The drug and target information were retrieved from the Drug Gene Interaction Database (DGIdb) (https://dgidb.org). The clinical trial stages of these drugs were obtained from the DrugBank database (https://go.drugbank.com/). Indications of licensed drugs and compounds under development were sourced from the ChEMBL database (https://ebi.ac.uk/chembl). All other data needed to evaluate the conclusions in this paper are present in the paper and/or the Supplementary Materials. The source codes pertaining to both the brain age estimation model and data analysis in this manuscript are provided on Zenodo repository at https://zenodo.org/records/14525707.

Submitted 27 June 2024
Accepted 4 February 2025
Published 12 March 2025
10.1126/sciadv.adr3757